Marine Micropaleontology 86–87 (2012) 15–31

Contents lists available at SciVerse ScienceDirect

Marine Micropaleontology

journal homepage: www.elsevier.com/locate/marmicro

Characterization of the Latest Danian Event by means of benthic foraminiferal assemblages along a depth transect at the southern Tethyan margin (Nile Basin, Egypt)

Jorinde Sprong [a], Tanja J. Kouwenhoven [a,*], André Bornemann [b], Peter Schulte [c], Peter Stassen [a], Etienne Steurbaut [a,d], Mohamed Youssef [e], Robert P. Speijer [a]

[a] Department of Earth and Environmental Sciences, University of Leuven, Celestijnenlaan 200E, 3001 Leuven, Belgium
[b] Institute of Geophysics and Geology, Leipzig University, Talstraße 35, 04103 Leipzig, Germany
[c] GeoZentrum Nordbayern, Universität Erlangen, Schloßgarten 5, 91054 Erlangen, Germany
[d] Royal Belgian Institute of Natural Sciences, Vautierstraat 29, B-1000 Brussels, Belgium
[e] Geology Department, Faculty of Science, South Valley University, 83523 Qena, Egypt

ARTICLE INFO

Article history:
Received 11 July 2011
Received in revised form 29 December 2011
Accepted 4 January 2012

Keywords:
Latest Danian Event
Southern Tethyan shelf
Benthic foraminifera
Depth transect
Hyperthermal
Sea level

ABSTRACT

The Latest Danian Event (LDE) has been recognized on the southern Tethyan margin (Egypt; Tunisia), and in the Atlantic (Zumaia, Spain) and Pacific Oceans (ODP Site 1209). Based on a supraregional carbon isotope excursion, and a negative shift in oxygen isotopes in the Pacific it has been suggested that the LDE is an early Paleogene transient warming event. So far the environmental effects of the LDE have been observed in few sections and details on its impact and duration are scarce. We present a quantitative study of benthic foraminiferal assemblages retrieved from five sections along a depth transect on the Paleocene southern Tethyan shelf (Nile Basin, Egypt) to assess paleoenvironmental change during the LDE. The lithologic sequences and foraminiferal assemblages indicate that the onset of the LDE is related to widespread shelf dysoxia. The organic-rich laminated marls of lower LDE bed I contain levels devoid of benthic foraminifera. During the later stage of the LDE (dark-gray shales of bed II) the shelf is repopulated by a *Neoeponides duwi* benthic assemblage, occurring in all sections, initiating a gradual restoration of normal-marine shelf environments. Q-mode and R-mode correspondence analysis assist in the interpretation of the *N. duwi* assemblage, which is related to disturbed conditions at the sea floor following oxygen depletion and increased organic loading. The sharp lithologic boundary at the base of the LDE suggests that the event coincides with a rapid transgression following a sea-level fall, with an estimated amplitude of ~50 m or less. Comparison with the Dan-C2 and ELPE/MPBE, two proposed transient warming episodes preceding and postdating the LDE, shows that the three Paleocene events have several characteristics in common. However, the duration of the LDE (~200 kyr) exceeds the estimated duration of the other events, and a sea-level cycle is only reported from the LDE.

1. Introduction

Studies of causes and consequences of the Paleocene–Eocene Thermal Maximum (PETM, around 55 Ma: e.g., Kennett and Stott, 1991; Dickens et al., 1997; Norris and Röhl, 1999; Thomas et al., 2002; Kent et al., 2003; Higgins and Schrag, 2006; Sluijs et al., 2007; Zachos et al., 2008) have led to a search for similar transient warming episodes, preceding and post-dating this globally impacting event. Several younger, early Eocene hyperthermals have been proposed and identified, such as the ETM-2 and 'X' events (e.g., Lourens et al., 2005; Nicolo et al., 2007; Agnini et al., 2009; Stap et al., 2009). It is likely that similar events preceded the PETM (e.g., Thomas and Zachos, 2000; Bralower et al., 2002), as these hyperthermals are probably triggered by astronomical forcing parameters (e.g., Cramer et al., 2003; Dinarès-Turell et al., 2003; Lourens et al., 2005; Westerhold et al., 2008, 2011; Lunt et al., 2011). Proposed Paleocene transient warming events are the early Paleocene Dan-C2 event (Quillévéré et al., 2002, 2008; Coccioni et al., 2010), and the Early Late Paleocene Event (ELPE: Petrizzo, 2005; Bralower et al., 2006), or Mid-Paleocene Biotic Event (MPBE, Bernaola et al., 2007).

A transient warming event, associated with sea-level change in Egypt around the Danian–Selandian transition (~61 Ma) was proposed because of sedimentologic and paleontologic similarities with

* Corresponding author. Tel.: +32 16 326452; fax: +32 16 322980.
E-mail addresses: Tanja.Kouwenhoven@ees.kuleuven.be (T.J. Kouwenhoven), a.bornemann@uni-leipzig.de (A. Bornemann), schulte@geol.uni-erlangen.de (P. Schulte), Peter.Stassen@ees.kuleuven.be (P. Stassen), etienne.steurbaut@naturalsciences.be (E. Steurbaut), myousefgeology@gmail.com (M. Youssef), Robert.Speijer@ees.kuleuven.be (R.P. Speijer).

0377-8398/$ – see front matter © 2012 Elsevier B.V. All rights reserved.
doi:10.1016/j.marmicro.2012.01.001

the PETM (Speijer, 2000, 2003a). Through a series of calcareous nannofossil-based cross-correlations between the North Sea Basin, SW France and the Tethys, Steurbaut and Sztrákos (2008) pointed out that this event occurred in the latest Danian, ca. 400 kyr prior to the originally defined Danian/Selandian boundary. Recently this event, referred to as the Latest Danian Event (LDE) was more accurately dated and evaluated (Bornemann et al., 2009; Sprong et al., 2009; Youssef, 2009; Sprong et al., 2011). Bornemann et al. (2009) compared shifts in benthic foraminiferal $\delta^{13}C$ and $\delta^{18}O$ with data from Zumaia (Schmitz et al., 1997, 1998; Arenillas et al., 2008) and ODP Hole 761B (Quillévéré et al., 2002; Quillévéré and Norris, 2003), and proposed a correlation with the 'top Chron C27n' event defined from a carbonate dissolution horizon observed at ocean drilling sites in the Atlantic and Pacific Oceans (Westerhold et al., 2008; Dinarès-Turell et al., 2010; Westerhold et al., 2011). This in turn is time-equivalent with the 'CIE-DS1' carbon isotope excursion at Zumaia (Spain: Arenillas et al., 2008; Dinarès-Turell et al., 2010; Westerhold et al., 2011). In a detailed study of benthic foraminifera, $\delta^{13}C$ and trace elements of the Qreiya 3 section (Eastern Desert, Egypt), Sprong et al. (2011) constrained the magnitude of the sea-level cycle associated with the LDE to a maximum of 50 m. The sea-level rise was found to be associated with anoxia at the sea floor and the subsequent incursion of a *Neoeponides duwi* assemblage, interpreted as repopulation of the sea floor.

The present study focuses on the Latest Danian Event (LDE) as recorded on the southern Tethyan epicontinental shelf, now exposed in the Eastern Desert in Central Egypt, where the LDE is recognized in several sections (Figs. 1 and 2).The aim is to explore and characterize the lateral extent of paleoenvironmental and faunal change during the LDE in the Eastern Desert by means of a quantitative analysis of benthic foraminiferal assemblages. A further objective is to evaluate sea-level change associated with the LDE. Furthermore, a comparison is made with the Dan-C2 and ELPE/MPBE events. We chose five sections along a paleobathymetric gradient on the southern Tethyan shelf, including the Qreiya 3 section studied by Sprong et al. (2011) as a reference section in the transect.

2. Studied sections and stratigraphy

2.1. Regional geologic background

The structural development of Egypt during the late Cretaceous and Paleocene was strongly influenced by the reactivation of fault systems originating in the Precambrian basement (Al Rifaiy and Cherif, 1987; Guiraud and Bosworth, 1999; Bauer et al., 2003). The main structural units controlling Paleocene sedimentation were the Arabian–Nubian massif in the south, the 'stable shelf' (Nile Basin) in central Egypt, and the 'unstable shelf' (Syrian Arc or Northern Egypt Basin) in the north (Figs. 1a, 2; Said, 1962, 1990; Shahar, 1994; Tawadros, 2001). During Danian–Selandian times (~65.5–58.7 Ma; Luterbacher et al., 2004), deltaic and coastal deposition (Kiseiba and Kurkur Formations.; Table 1) and phases of erosion characterized the southern margin of the Basin, which was situated close to the present southern border of Egypt (Luger, 1985, 1988; Hendriks et al., 1987; Hewaidy, 1994). In most of the area north of Aswan, hemipelagic marl and clay deposition prevailed in a generally northward deepening basin. Uplifted areas were the Syrian Arc in northern Egypt ('unstable shelf' of Said, 1962, 1990; e.g., the Galala platform: Scheibner et al., 2003; Table 1) and the local high of Abu Tartur in central Egypt (Schnack, 2000) (Figs.1, 2). Whereas the 'unstable shelf' to the north was influenced by tectonic activity, the Nile Basin experienced little structural deformation during the early Paleogene (Shahar, 1994). This structural quiescence, together with relatively low rates of subsidence, favored deposition of a more or less continuous succession of marine sedimentary facies over large areas. Various studies suggest that a fairly complete upper-lower Paleocene to lower Eocene stratigraphic record is present in large parts of Egypt (e.g., Said, 1990).

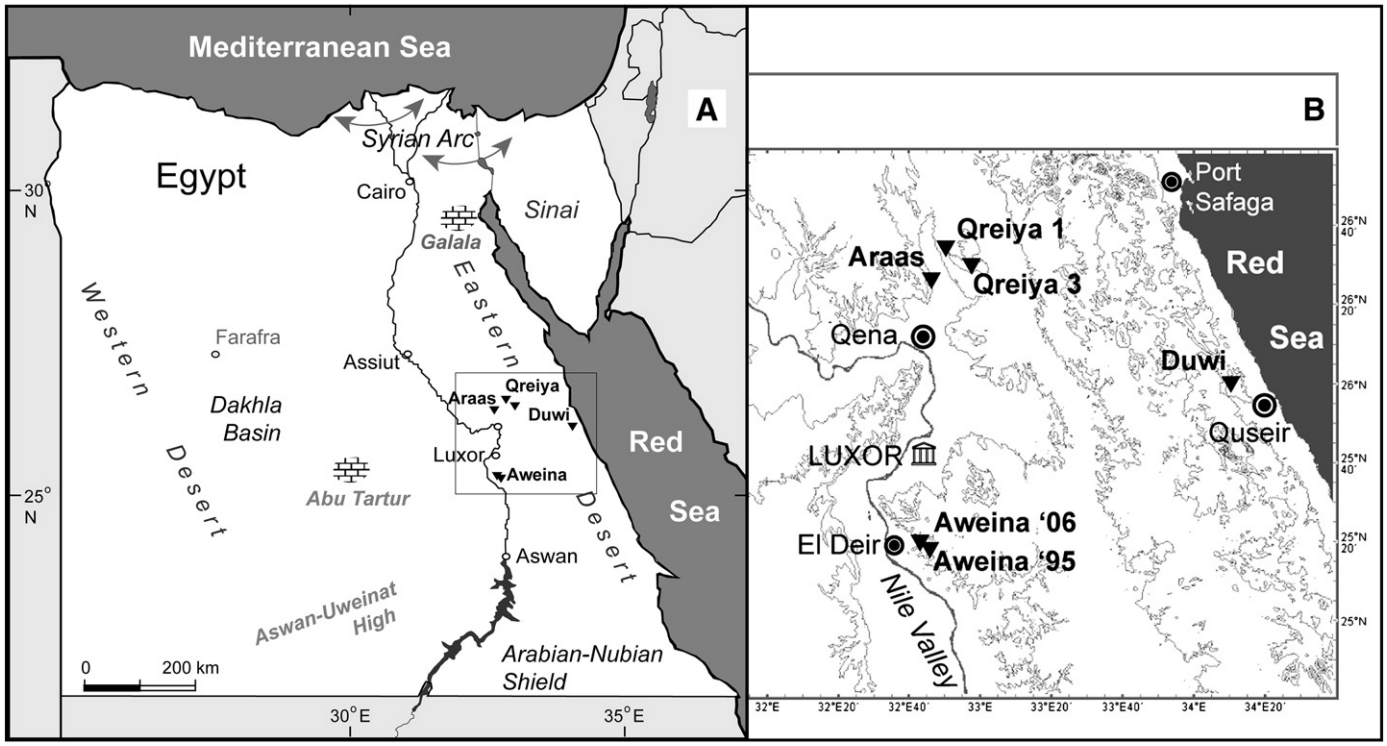

Fig. 1. Maps of the study area. A: General map of Egypt, indicating the 'stable shelf', the 'unstable shelf', and the Eastern Desert. B: Close-up of panel (A) showing the locations of the sections studied in the Eastern Desert. Araas: 26° 22′ 24″ N 32° 45′ 37″ E; Aweina (sampled in 1995): 25° 14′ 17″ N 32° 46′ 48″ E; Aweina (sampled in 2006): 25° 14′ 39″ N 32° 46′ 00″ E; Duwi: 26° 06′ 06" N 34° 06′ 46″ E; Qreiya 1: 26° 30′ 11″ N 32° 52′ 18″ E; Qreiya 3: 26° 27' 42″ N 33° 01′ 54″ E.

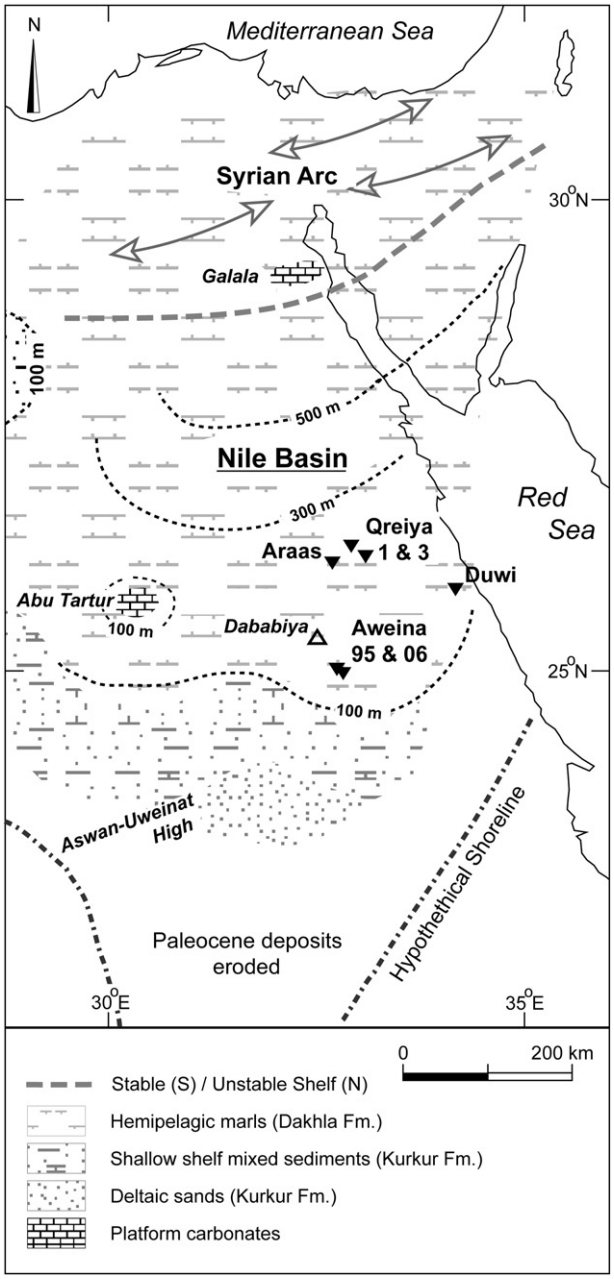

Fig. 2. Paleogeographic map of the Eastern Desert, with paleobathymetric contour lines. Modified from Speijer (2003a).

The Dakhla Formation (Fm.) is of late early Maastrichtian to early late Paleocene age and attains a thickness of up to 130 m in the Eastern Desert (Hendriks et al., 1987). This formation consists of rather monotonous brownish to grey marls and shales. The open marine strata of the Dakhla Fm. have accumulated in shelf environments of the Nile Basin peripheral to the Tethys Ocean in the North (Hendriks et al., 1987; Mart, 1991; Table 1). The LDE beds are intercalated in the Dakhla Fm. The sections in which the LDE is studied are located in the Eastern Desert (Fig. 1), close to the northwestern margin of the Arabian–Nubian shield, on the stable shelf (Bartov and Steinitz, 1977; Said, 1990). In the studied time interval, the sections were arranged along a paleobathymetric gradient (Fig. 2; see also Speijer, 2003a). Benthic foraminifera from Danian and Selandian marly and shaly sediments of the basin reflect middle to shallow-outer neritic shelf depths (70 to 150 m) at Gebel Duwi. At the deeper end of the transect, in the Qreiya sections, the faunas are typical of the deep outer shelf/upper slope (150 to 250 m: Speijer, 2003a; Sprong et al., 2011); probably some 100 m deeper than the Duwi section.

2.2. Sections and sampling

Five sections were (re-) sampled in 2006 with focus on the LDE beds. The Qreiya 3 section is situated east of the southern entrance of Wadi Qena, 45 km northeast of the town of Qena. The Qreiya 1 section is situated ~15 km to the west-northwest of Qreiya 3. The Araas section is also situated in the Wadi Qena area, ~20 km southwest of Qreiya 1 and ~20 km north of Qena. The Aweina section sampled in 1995 is located 15 km east of the Nile River, ~20 km east-southeast of the town of Esna. The detailed sample set of 2006 was collected 1.5 km north of this section from a 60 cm thick interval around the LDE beds. The Duwi section is located in the vicinity of the Red Sea coast, 16 km west of the coastal town of Quseir (Kosseir). At Duwi a detailed sample set across the LDE was collected in 2006 on the same outcrop as sampled in 1995.

In order to obtain fresh rock, the samples were collected from 10 to 30 cm deep trenches or holes along the outcrops. Burrows and redeposited sediments visible in the outcrop were as much as possible avoided during sampling. Sample spacing varies from 1 m over parts of some of the longer sequences to 1 cm across the LDE beds.

2.3. Lithology of the LDE beds

Except for the Duwi section, the sequences show a similar lithostratigraphy across the LDE including two main cm- to dm-thick event beds. The lower event bed consists of purplish-brown, laminated shales rich in organic material, whereas the upper event bed consists of dark-gray, marly shales. The thickness of both beds is variable (Figs. 3, 4). The contact of the lower bed with the underlying Dakhla shales is sharp in all sections, whereas the upper transition is gradual.

In the Qreiya 1 section the total thickness of the LDE beds is 12 cm. The laminated, dark brown-purplish marls of LDE Bed I (2 cm thick) occur 4.10 m above the base of the sampled section and are rich in fish remains and nodules, possibly representing coprolites. Just below, and within Bed I, planktic foraminifera are nearly absent. The top cm of Bed I contains abundant, often pyritized planktic foraminifera. Between 4.12 and 4.18 m, dark gray shales of Bed II are exposed, containing gastropod molds and very few planktic foraminifera. The top 4 cm of Bed II are thinly interlayered, dark gray shales and dark purplish brown marls which seem to consist partially of redeposited sediments of Bed 1. They contain clay pebbles, fish remains and a level with abundant pyritized planktic foraminifera.

The LDE beds in the Qreiya 3 section attain a thickness of ~25 cm and form a prominent ridge in the outcrop. The base of the LDE is situated 8.20 m above the base of the sampled section. The gray marls below the event beds (8.05–8.20 m) are darker, and mottled just below the contact with the LDE. Extremely low numbers of calcareous microfossils and low calcium carbonate content in these marls are attributed to dissolution (Sprong et al., 2011). LDE Bed I (~10 cm thick) consists of dark purplish-brown laminated marls and is rich in organic material. Bed I contains abundant fish remains and planktic foraminifera, of which many are pyritized. Benthic foraminifera are absent from the lowermost 3 cm. Burrows excavated downward from LDE Bed II, showing as dark-gray clay lenses parallel with the laminations in the upper 7 cm, contain benthic foraminifera. LDE Bed II (~15 cm thick) is gray to dark-gray marly shale containing hematitic and limonitic bivalve and gastropod molds. Purplish-brown marl, bioturbated upward from Bed I is found in the lower part of Bed II. Overlying the dark gray shales of Bed II are a few cm of a partially layered admixture of dark gray shales and brownish marls which, as in Qreiya I, might represent redeposited sediments.

A short, continuously exposed sequence of 2.85 m was studied in the Araas section, starting 35 cm below the base of the LDE beds.

Table 1
Overview of correlative lithologic formations in Egypt, with local names.

		S — WESTERN DESERT — N							
		Bir Murr - Bir Dungul Luger, 1985, 1988	**W. Abu Ghurra** Youssef, 2003	**S- Kharga** El-Azabi and Farouk, 2011	**N- Kharga** Schnack, 2000	**Abu Tartur** M. Hermina in Said, 1990	**Dakhla Basin** Schnack, 2000	**Farafra area** M. Hermina in Said, 1990	**N- W. Desert** G. Hantar in Said, 1990
Eocene		Dungul Fm	Dungul Fm	Dungul Fm	Thebes Fm	Dungul Fm	Thebes Fm	Naqb Fm	Apollonia Fm
Paleocene	Upper	Garra Fm / Kurkur Fm	hiatus / Garra Fm	hiatus / Garra Fm	Esna Fm / Tarawan Fm	Garra Fm / Kurkur Fm	Esna Fm / Tarawan Fm	Esna Fm / Tarawan Fm	
		hiatus	hiatus	hiatus	hiatus	hiatus	hiatus	hiatus	
	Lower	Kurkur Fm	Kurkur Fm / hiatus / Dakhla Fm	Kurkur Fm	Dakhla Fm	Kurkur Fm	Dakhla Fm	Dakhla Fm / Khoman Fm	
		hiatus	hiatus	hiatus	hiatus	hiatus	hiatus	hiatus	hiatus
U. Cretaceous	Maastr.	Kiseiba Fm: Shab Mb	Dakhla Fm	Dakhla Fm	Dakhla Fm	Dakhla Fm	Dakhla Fm	Khoman Fm	Khoman Fm
		Kiseiba Fm	Kiseiba Fm	hiatus					
	Camp.	Shagir Mb		Duwi Fm	Duwi Fm	Duwi Fm	Duwi Fm	El Hufuf Fm	Abu Roash Fm

		S — EASTERN DESERT - SINAI — N				
		Red Sea coastal plain R. Said in Said, 1990	**Nile Valley Basin** R. Said in Said, 1990	**Galala area** Scheibner et al., 2003 *Platform*	*Slope*	*N- E. Desert*	**Unstable Shelf** R. Said in Said, 1990 *N- Eastern Desert*
Eocene		Thebes Fm	Thebes Fm		Thebes Fm		Thebes Fm
Paleocene	Upper	Esna Fm / Tarawan Fm	Esna Fm / Tarawan Fm	S. Galala Fm	S. Galala Fm	Esna Fm / Tarawan Fm	Esna Fm
	Lower	Dakhla Fm Beida Mb	Dakhla Fm	St. Anthony Fm	Dakhla Fm	Dakhla Fm	
		hiatus	hiatus	hiatus			hiatus
U. Cretaceous	Maastr.	Dakhla Fm Hamma Mb	Dakhla Fm	St. Anthony Fm	Sudr Fm		Sudr Fm
	Camp.	Duwi Fm	Duwi Fm				

The thickness of the LDE deposits is 10 cm. The 8 cm thick interval below the event beds consists of dark gray shales; the upper 4 cm of this interval contain no planktic or calcareous benthic foraminifera. Bed I (~5 cm thick) consists of brown-purplish marl with fish remains (scales and coprolites) and levels with abundant pyritized planktic foraminifera. Between 2 and 5 cm the marl is laminated, and contains thin slivers of dark gray clay interpreted as burrows, bioturbated in from above. Between 5 and 7 cm the brown-purplish marl is thinly interlayered with dark gray shale. Bed II, between 7 and 10 cm, consists of dark gray shaly marls grading upward into lighter gray marls typical of the Dakhla Fm.

At Gebel Aweina, the Danian–Selandian succession is most expanded. A sequence of 20 m was studied of the section sampled in 1995 (Aweina '95; this section was studied at low resolution by Speijer and Schmitz (1998)), from 16 to 36 m above the K/Pg boundary. The LDE, recorded at 26 m, was sampled in detail in 2006 in a parallel section spanning 60 cm (Aweina '06). LDE Bed I (~3 cm thick) consists of laminated dark brown-purplish marls with coprolites and the top contains high numbers of, mostly pyritized, planktic foraminifera. Burrows penetrate a few cm into the underlying gray marls, where numbers of planktic and calcareous benthic foraminifera are extremely low. LDE Bed II (~2 cm thick) is dark gray shale with pyrite nodules, and remains of bivalves and gastropods.

About 11 m of the Duwi section was studied, between 32.6 and 43.2 m above the K-Pg boundary. The LDE at Gebel Duwi is developed as a ~10 cm thick light gray, upwards fining marl bed containing fish remains, coprolites and burrows penetrating into the underlying gray marls. The lower 5 cm of the marl bed are laminated. At ~5 cm a gypsum layer occurs. The LDE bed is underlain and overlain by gray shaly marls, at some levels containing numerous small burrows and fish remains.

2.4. Biostratigraphy

The planktic foraminifer biostratigraphy is taken from Sprong et al. (2009, 2011), applying the biozonation criteria of Berggren and Pearson (2005). Most of the sections include planktic foraminiferal Zones P2 and P3 (Fig. 3). The studied parts of the Qreiya 3 and Duwi sections may range into the lower part of Zone P4. The P1/P2, and P2/P3 Zonal boundaries are delineated by the Lowest Occurrences (LOs) of *Praemurica uncinata* and *Morozovella angulata,* respectively. The LO of *Igorina albeari* delineates the P3a/P3b sub-zonal boundary. The typical, large *Globanomalina pseudomenardii* (Olsson et al., 1999), the LO of which delineates the P3/P4 Zonal boundary, was not found. Small *Globanomalina* specimens (<125 μm) are referred to as *G.* cf. *pseudomenardii* and their LO is indicated by a small arrow (Fig. 3). In the Qreiya 3 and Duwi sections the LO of *M. velascoensis* is indicated by a bold arrow. In the Aweina section the LO of *M. velascoensis* is found 1 m above the top of the studied section. Speijer (2003a) used this taxon to approximate the P3/P4 Zonal boundary; however, in deep-sea sections the LO

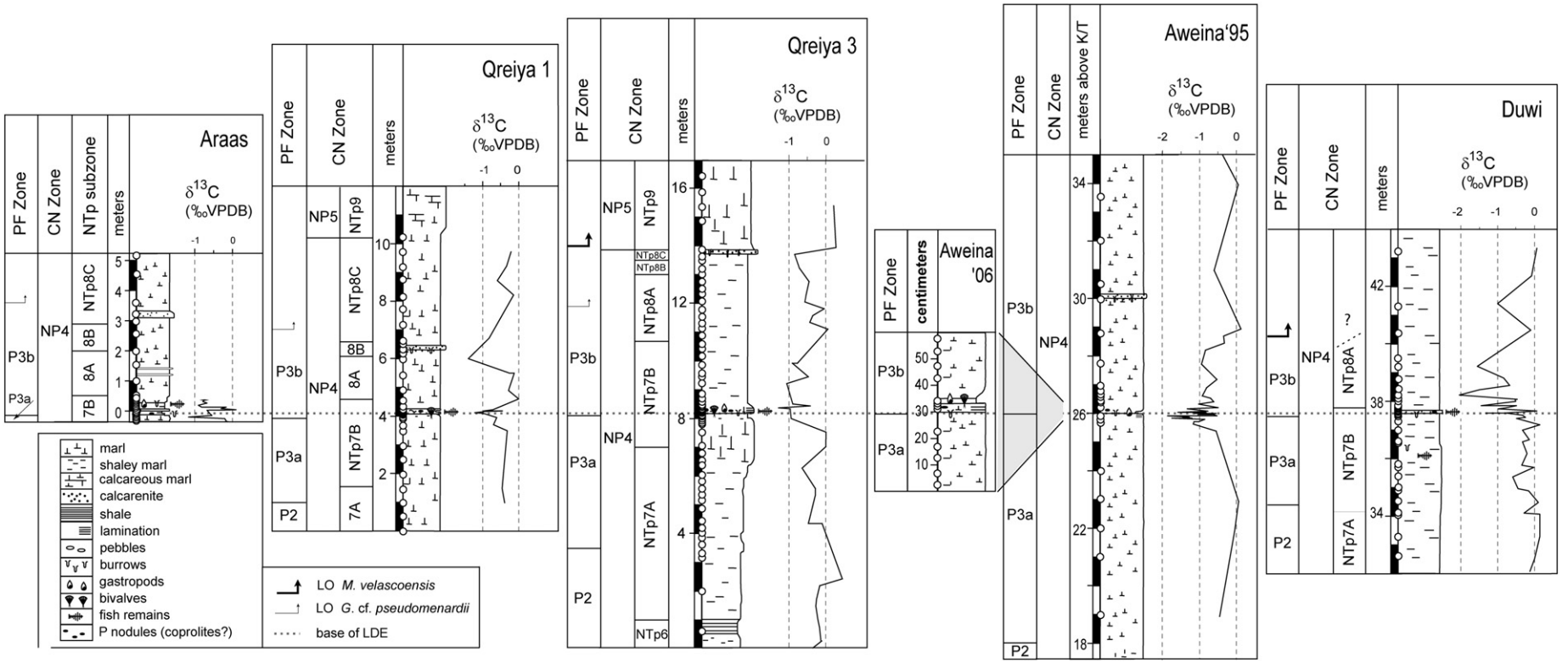

Fig. 3. Lithology and biostratigraphy of the sections, with benthic foraminiferal $\delta^{13}C$ records from Bornemann et al. (2009). The $\delta^{13}C$ data of the Araas section are new. PF (planktic foraminiferal) Zones after Berggren and Pearson (2005). CN (calcareous nannofossil) Zones after Martini (1971). NTp (calcareous nannofossil) Subzones after Varol (1989). Biostratigraphy is taken from Sprong et al. (2009) and Youssef (2009). Open circles represent sample points.

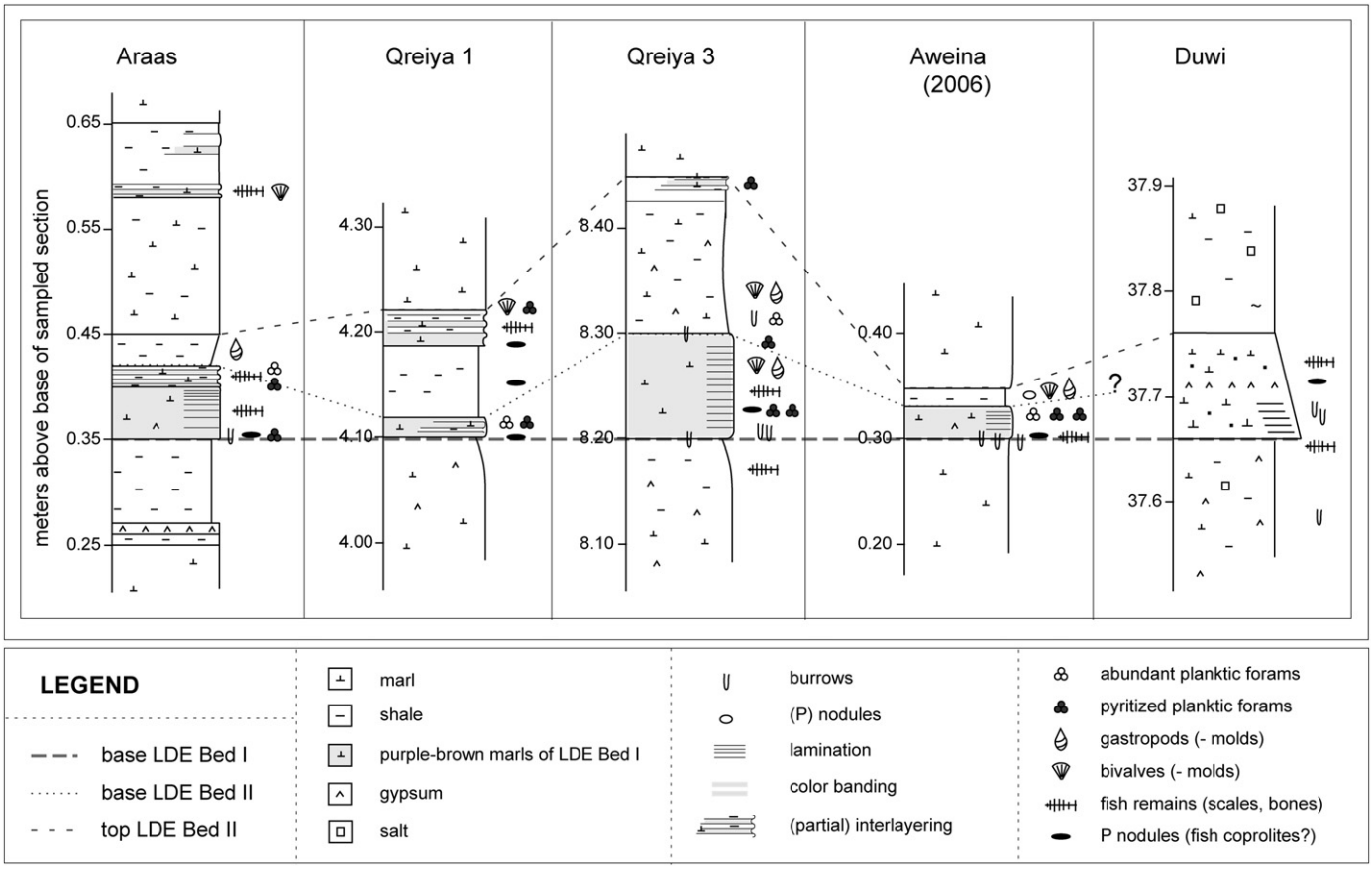

Fig. 4. Detailed lithology of the event beds of the five studied sections. Correlation lines indicate the base of LDE Bed I, and the base and the top of LDE Bed II.

of *M. velascoensis* is consistently found in Zone P3b (e.g., Olsson et al., 1999; Wade et al., 2011).

The calcareous nannofossil zonation follows Martini (1971) and Varol (1989). For the Qreiya 3 section the zonation is based on Sprong et al. (2011); for the other sections on Youssef (2009). All sections include part of Zone NP4. The Qreiya 1 and 3 sections also include the NP4/NP5 boundary, delineated by the LO of *Fasciculithus tympaniformis*, and the lower part of Zone NP5. The (sub-) zonal boundaries are delineated by the highest occurrence (HO) of *Neochiastozygus eosaepes* (NTp6/NTp7), and the successive LOs of *Chiasmolithus edentulus* (NTp7A/NTp7B), *Sphenolithus primus* (NTp7/NTp8), *Fasciculithus billii* or *F. ulii* (NTp8A/NTp8B), and *F. janii* or *F. pileatus* (NTp8B/NTp8C).

3. Methods

For each sample, about 50 g of sediment was dried at 60 °C for 24 h, weighed, disintegrated in a soda solution (50 g/L Na_2CO_3) and washed over a set of 2 mm and 63 μm sieves. Burrows and reworked/redeposited layers visible in the sample material were to the maximum possible extent separated from the rest of the material. The residues were dry-sieved over 630 and 125 μm sieves. The fraction 125–630 μm was used for quantitative analyses. Representative aliquots preferably containing 200 or more specimens were obtained with an ASC microsplitter (Appendix A). Foraminifera were hand-picked from the washed residues, transferred to micropaleontologic slides, and stored in the collection of R.P. Speijer at the Department of Earth and Environmental Sciences, K.U.Leuven (Belgium) for future reference. Preservation of the samples was fairly good in most samples (taxonomy not problematic) to poor (mainly samples with >50% non-calcareous agglutinated taxa from dissolution intervals). Most foraminifera were identified at species level, some at generic level (e.g., lenticulinids, and nodosariids). Counts of *Bulimina strobila* and *B. farafraensis* were taken together, as these species appear to intergrade. The non-calcareous agglutinated taxa (NCA: a group containing among others *Haplophragmoides* and *Trochammina* spp.) were placed in a supra-generic category, as poor preservation of these taxa often precluded more rigorous identification. The counts were transferred to relative frequencies.

Numbers of planktic (PFN) and benthic foraminifera (BFN) per gram of dry sediment were determined and the Shannon diversity index [H] was calculated (Shannon and Weaver, 1949; Spellerberg and Fedor, 2003). The P/B ratio, the ratio between planktic and benthic specimens present in a sample, was counted from random squares in the picking tray, and is expressed as $\%P = 100 \times P/(P + B)$. In open marine environments the P/B ratio is often used as a first estimate of paleobathymetry (Berger and Diester-Haass, 1988; Van der Zwaan et al., 1990). In addition, the benthic species were attributed to different water-depth categories based on empirically derived distribution patterns and literature sources (Table 2). The relative frequencies of species occurring in the same depth categories were summed in order to obtain insight into bathymetric differences between sections, and water-depth changes within sequences. The transition from neritic to bathyal is taken at ~200 m (cf. Van Morkhoven et al., 1986; Speijer, 2003a). The terms inner neritic (IN), middle neritic (MN), and outer neritic (ON) are used for paleodepths of <50 m, 50–100 m, and 100–200 m respectively (cf. Speijer, 2003a).

PAST computer software (Hammer et al., 2001) was used to run Q-mode and R-mode correspondence analyses (CAs) on the relative

frequency data. The complete data sets contain 87 taxa and 197 samples (Appendix A). For the CA the data of the Aweina sections sampled in 1995 and 2006 were combined. Rare species (single and scattered occurrences and species not occurring in relative frequencies ≥2% in at least one sample) were omitted. Excluded from CA were barren samples, samples collected in channel deposits and samples likely containing redeposited sediment or burrows. In addition, samples showing clear signs of dissolution were removed from the data set; for practical reasons, we removed those samples containing ≥25% non-calcareous agglutinated (NCA) taxa. The reasoning behind this is that excessive enrichment of the NCA taxa may point to dissolution of carbonate (e.g., Nguyen et al., 2009), whereas moderate enrichment of these taxa may be an ecologic phenomenon, associated with conditions of low oxygenation and variable organic flux (e.g., Kuhnt et al., 1996). Extra CA runs excluding ≥10% or ≥50% of the NCA taxa give approximately the same result (not shown). All remaining samples containing ≥150 specimens were included in CA; this number was chosen to keep as many samples as possible without compromising the analyses.

The CA was run on 62 taxa and 173 samples. Q-mode CA on the samples was run on the sections separately. For the R-mode CA run on the species, the data of all sections were combined.

For the Araas section, $\delta^{13}C$ analyses on *Pyramidulina* species were performed at the University of Erlangen, Germany (Fig. 3; Appendix B; for methods see Bornemann et al., 2009). Unfortunately these species were too scarce and too poorly preserved in the Araas section to create a complete $\delta^{13}C$ record.

4. Results

4.1. Benthic foraminiferal distribution and paleobathymetry

4.1.1. Benthic foraminiferal assemblages and paleodepth

The distribution through time of selected species is plotted per section, next to the distributions of the species groups summed per depth category (Fig. 5A, B; Table 2). Background samples below and above the LDE in the sections Qreiya 1, Qreiya 3, and Araas contain most bathyal benthic foraminifera (15–20%, including *Gavelinella beccariiformis*, *Nuttallides truempyi*, *Gyroidinoides globosus*, *Alabamina* cf. *A. creta*), whereas the percentage of middle to outer neritic taxa is <45–50%. The Aweina '95 section contains ≤10% bathyal taxa. In the Duwi section a small number (<5%) of bathyal taxa is restricted to the base of the sampled section, and middle to outer neritic taxa dominate the assemblage (~80%, including *Alabamina midwayensis*, *Anomalinoides affinis*, *A. midwayensis*, *Hansenisca girardanus*, *Oridorsalis plummerae*). Based on the relative abundances of depth categories of benthic foraminifera in Fig. 5(A, B), the studied sections represent a depth transect ranging between outer neritic to upper bathyal (Araas, Qreiya 1 and 3: ~150–250 m), and middle to outer neritic (Duwi: ~70–150 m). Aweina was situated at an intermediate, outer neritic paleodepth (150 to 200 m). This is in agreement with paleobathymetric trends outlined earlier (Speijer, 2003a; see Fig. 2). The P/B ratios do not reflect these depth differences, but vary between 70 and 95%P in all sections.

4.1.2. Dissolution intervals

Carbonate-poor levels were recognized in outcrops of the Araas and Qreiya 3 sections. Samples from these levels are characterized by low-diversity benthic assemblages dominated by, or almost exclusively consisting of non-calcareous agglutinated (NCA) taxa (predominantly trochamminids and *Haplophragmoides* spp.). In the Qreiya 3 section a carbonate-poor level is present below the LDE, whereas in the Araas section such levels occur below and above the LDE. In the Qreiya 1 and Aweina sections carbonate-poor levels were not recognized in outcrop, but in the Aweina section the NCA taxa dominate the benthic foraminiferal assemblages just below the LDE (50–70%). In the Qreiya 1 section the NCA taxa are less dominant, and one peak of 25% occurs at 4.18 m, within the LDE. In the Duwi section such levels heavily dominated by NCA taxa are absent.

4.1.3. Benthic foraminifera in the LDE

The benthic foraminiferal assemblages change significantly towards the LDE (Fig. 5A, B). In the deeper sections of the transect (Qreiya 1 and 3 and Araas sections) the deeper-water taxa disappear sequentially below the LDE. First to disappear are the bathyal taxa (*G. beccariiformis*, *N. truempyi*), followed by taxa with an outer-neritic to bathyal distribution (e.g., *Angulogavelinella avnimelechi*; *Anomalinoides affinis*; *Osangularia plummerae*) and those with an outer neritic distribution (e.g., *Cibicidoides pseudoacutus*, *C. rigidus*). In the interval where bathyal taxa disappear, *Siphogenerinoides esnehensis* and *Bulimina strobila* increase in abundance. *Neoeponides duwi* appears quite abruptly within the LDE beds in the Aweina, and Qreiya 1 and 3 sections. In the Duwi and Araas sections, the influx of *N. duwi* associated with the LDE starts slightly below LDE Bed I. However, some reworking cannot be excluded, despite the effort to avoid burrows and reworked sediments during sampling and sample processing. The relative abundance of *N. duwi*, associated with *Siphogenerinoides esnehensis*, costate lenticulinids, and *Bulimina strobila* temporarily increases to 50–80% in LDE bed II at the expense of the outer neritic taxa. This apparent shallowing is reflected in the low Shannon diversity index. Planktic and benthic foraminiferal numbers (PFN, BFN) show repeated shifts. A level barren of in-situ benthic foraminifera occurs in most sections in association with LDE Bed I. Above the LDE the benthic foraminiferal assemblages are gradually restored. Local extinctions are not recorded. The more expanded sections (Qreiya, Duwi, and to a lesser extent Aweina) show increasing abundances of buliminids towards the top of the sampled intervals (Fig. 5A, B).

4.2. Correspondence analysis

In the Q-mode correspondence analysis (CA), run on the samples of each of the sections separately, about 45% of the variance in the benthic foraminiferal data is explained by the first two CA axes (Fig. 6; Appendix C). The Q-mode CA distinguishes four main biofacies containing different foraminiferal assemblages: (1) an outer neritic to upper bathyal assemblage restricted to the Araas, Qreiya 1 and Qreiya 3 sections, and containing 10–20% of the upper bathyal taxa *G. beccariiformis* and *N. truempyi*; (2) an assemblage, present in each of the sections, containing typical middle to outer neritic taxa (e.g., *Alabamina midwayensis*, *Cibicidoides* spp. (among others *C. pseudoacutus*, *C. rigidus*), *Hansenisca girardanus*), and not containing the bathyal taxa; (3) a middle to outer neritic assemblage containing 10–25% buliminids, present well above the LDE in all sections except Araas, which is probably too short to record this interval; (4) a middle neritic assemblage, dominating within the LDE interval in all sections. In the shallower Aweina and Duwi sections, the samples collected in the lithological LDE (assemblage 4A) group together within a larger group of samples composed of inner to middle neritic assemblages. Assemblage 4 shows virtually no overlap on the first CA axis with the other groups of samples, containing the middle to outer neritic and outer neritic to bathyal assemblages.

Of the R-mode CA, run on species of all sections together, only the most informative taxa are shown (Fig. 7A). The first two axes of the R-mode CA explain ~34% of the variance in the data set. On the first CA axis the bathyal taxa *G. beccariiformis* and *N. truempyi* are positioned opposite the inner to middle neritic taxon *N. duwi*. *Siphogenerinoides esnehensis* groups with the buliminids at the negative side of the second axis, and on both axes opposite *S. elegantus*, the smoother morphotype of *Siphogenerinoides*. The non-calcareous agglutinated (NCA) taxa, which were only considered in abundances ≤25%,

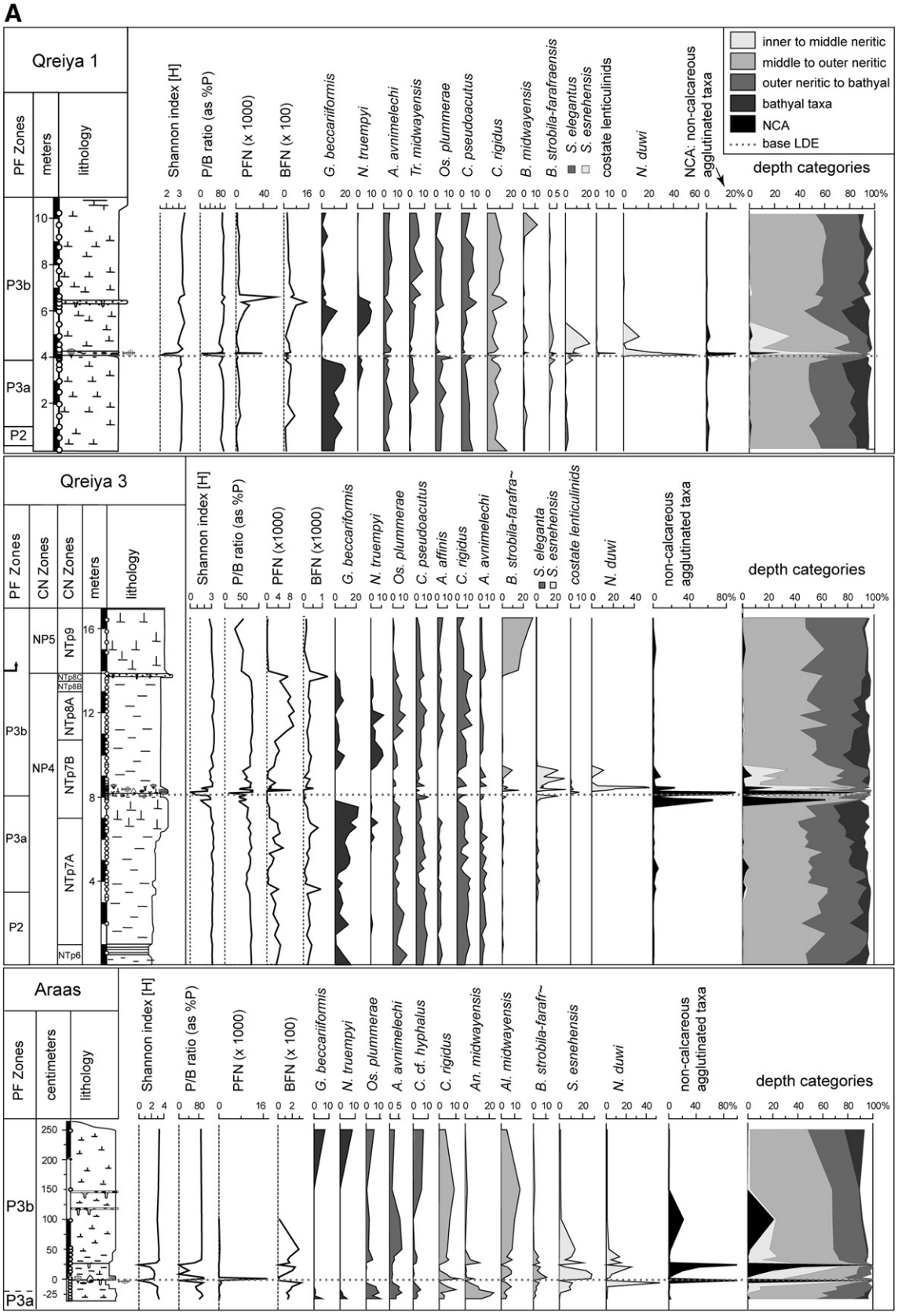

Fig. 5. Benthic foraminiferal data. To the left: planktic foraminiferal numbers (PFN), benthic foraminiferal numbers (BFN), Shannon diversity index [H], and P/B ratio, expressed as %P. Middle: relative abundances of selected taxa. To the right: relative abundances summed per bathymetric group. A: Qreiya 1, Qreiya 3 and Araas sections. B: Aweina '95, Aweina '06 and Duwi sections. Open circles represent sample points.

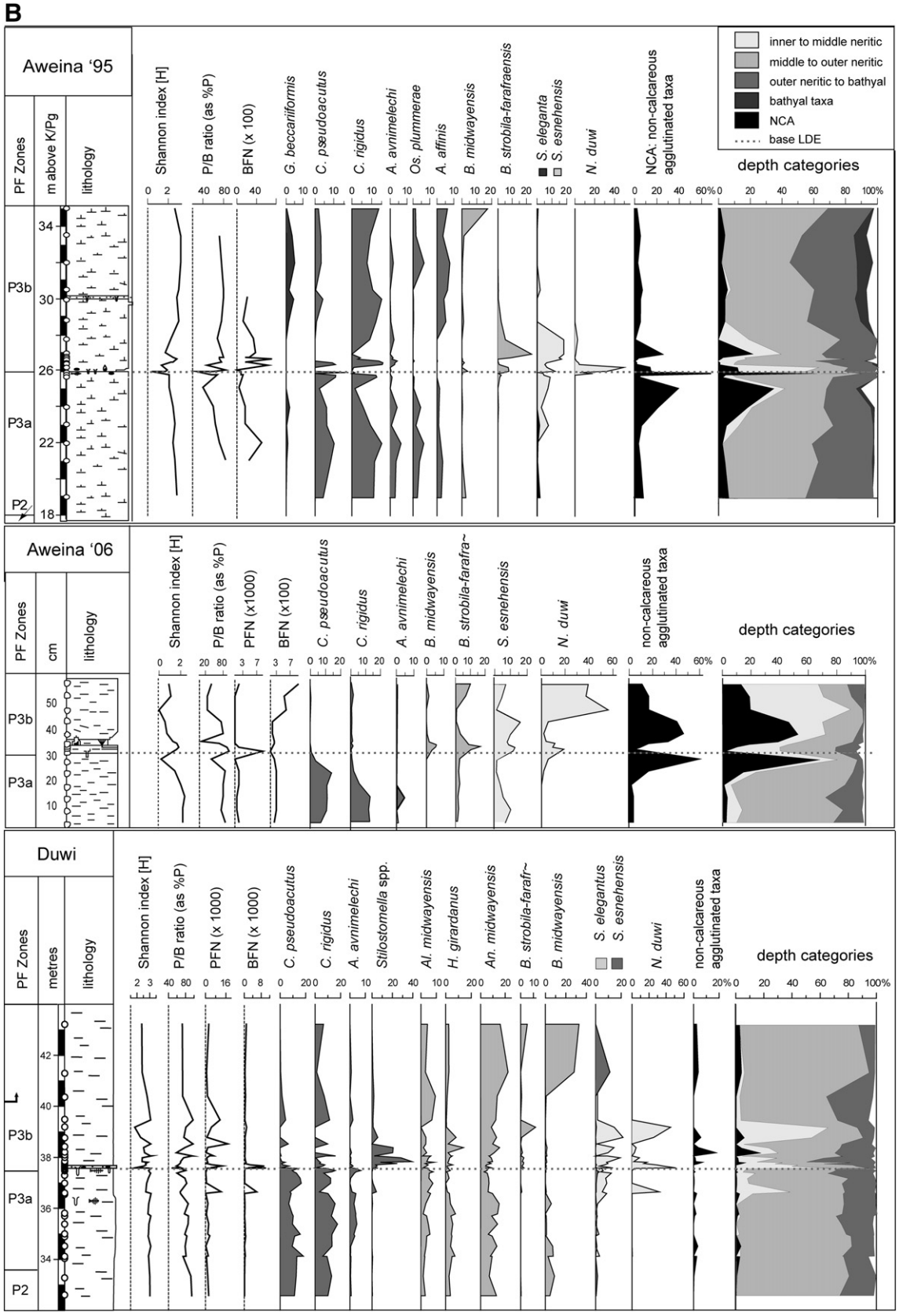

Fig. 5 (*continued*).

group between *N. duwi* and the buliminids on the first axis. On the second CA axis their position is just on the negative side. The environmental interpretation (Fig. 7B) is based on this distribution of the species on the CA axes, and on the CA scores (Appendix C), together with information about their depth distributions (Table 2; see Section 5.2.2 for discussion).

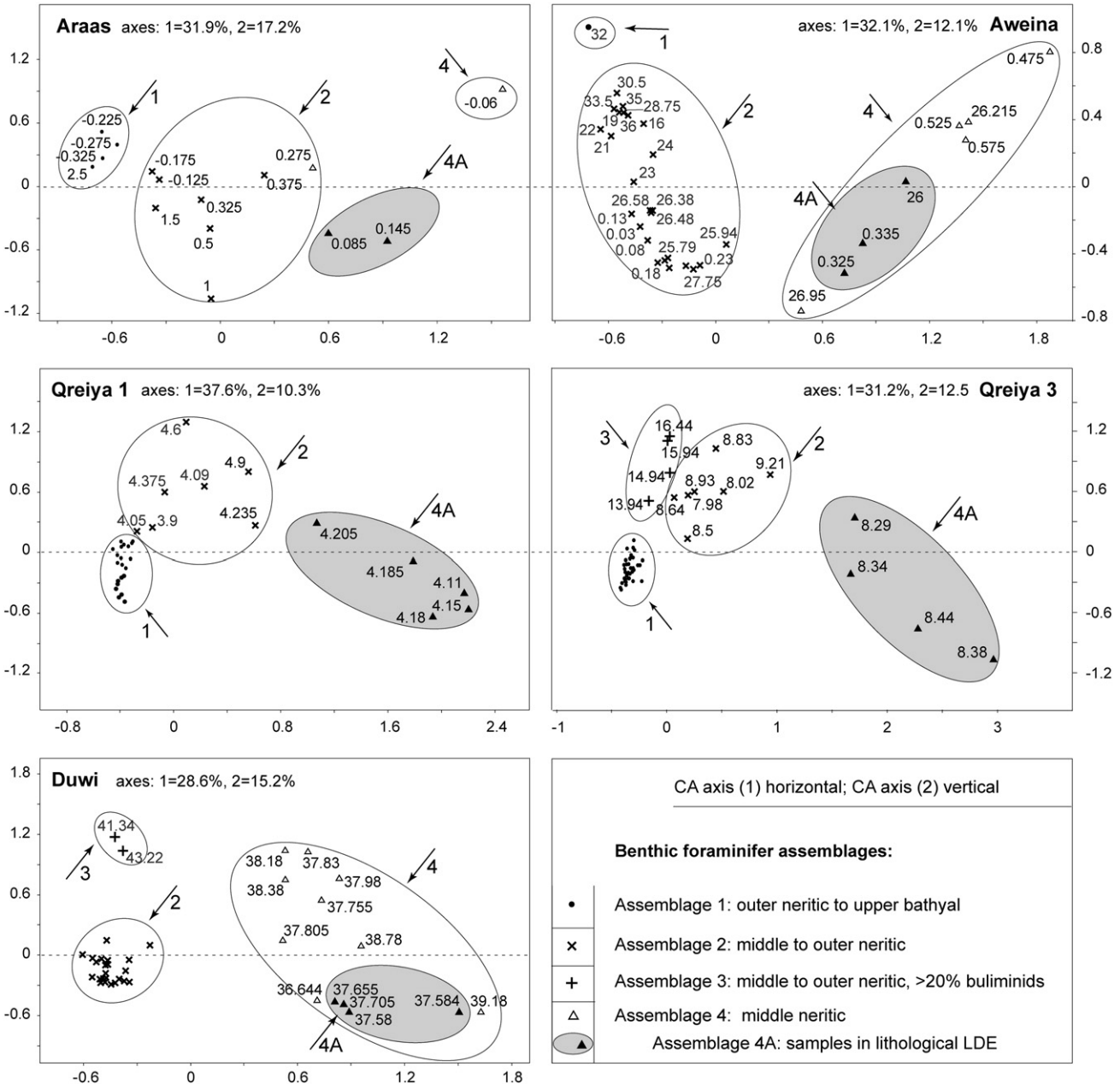

Fig. 6. Q-mode correspondence analysis. The sections were analyzed separately. Horizontal: CA axis 1, vertical: CA axis 2. Percentage of variance explained by the CA axes is given. Four assemblages are distinguished by CA. For discussion see text.

5. Discussion

5.1. Dissolution horizons

Calcium carbonate-poor levels are present below and within the LDE beds (see Section 4.2.2). The low calcium carbonate content, together with low foraminiferal diversity, and dominance of non-calcareous agglutinated (NCA) foraminifera (Fig. 5A, B), provides clear evidence of syn- or postdepositional carbonate dissolution. The presence of gypsum and/or anhydrite points to alteration of pyrite. Possible causes of carbonate dissolution include acidification of pore waters by high organic load, pyrite alteration, and downward migration of a redox front (comparable to the 'burning-down' of sapropels: e.g., Higgs et al., 1994; Thomson et al., 1995). Consequently, we do not include these levels in the LDE; contrary to Soliman and Obaidalla (2010), who include a dark clay bed underlying the purplish-brown marl in their 'el Qreiya beds', the equivalent of the LDE.

Carbonate-poor levels are not present in the Duwi section, nor are samples dominantly containing NCA taxa. The deviating lithologic expression of the LDE in the Duwi section may be related to the shallower depositional depth and a different paleoenvironmental setting. Alternatively, the actual LDE beds might have been eroded, and reworked into the upwards-fining light-gray marls, which would be in line with our observations of erosional channels cutting through the LDE in the outcrop of the Qreiya 3 section (Sprong et al., 2011).

5.2. Sea-floor oxygenation and eutrophication

5.2.1. Lithology and geochemistry

With the exception of the Duwi section, the LDE interval shows a similar lithological expression in all studied sites (Section 2.2; Fig. 4). Evidence for dys- or anoxia is limited to LDE bed I, and includes fine sedimentary laminations, preservation of fish remains,

Table 2
Depth distributions of taxa. References: 1 – Speijer and Schmitz, 1998; 2 – Schnack, 2000; 3 – Ernst et al., 2006; 4 – Stassen et al., 2009. Correspondence analysis (CA) scores of the first two axes are given. IN: inner neritic; MN: middle neritic; ON: outer neritic; B: bathyal. Solid line: common occurrence; dashed line: occasional occurrence. Asterisk: own observations.

	CA axis 1	CA axis 2					
taxa	24.70%	9%	**IN**	**MN**	**ON**	**B**	ref.
agglutinated sp. B	0.020269	-0.26768					
agglutinated sp. C	-0.53425	-0.07966					
Alabamina creta	-0.38697	-0.09159				—	1
Alabamina midwayensis	-0.035059	-0.29423	- - - -	———		- - - -	1-4
Ammodiscus cretaceus	-0.1199	-0.31595		———			1,2
Angulogavelinella avnimelechi	-0.42082	0.13792			———		1,3,4
Anomalinoides affinis	-0.57364	0.19458			———		1,2,4
Anomalinoides midwayensis	-0.10396	-0.20686	———	———			2,4
Anomalinoides praeacutus	-0.28225	-0.18989		———		- - - -	1,2,4
Anomalinoides rubiginosus	-0.4982	0.17298		- - - -	—	- - - -	1,2
Anomalinoides susanaensis	-0.63657	0.58089			—	- - - -	1,2
Bulimina midwayensis	-0.14611	-0.27944	- - - -	———		- - - -	1-4
Bulimina ovata-quadrata	-0.047121	-0.32455	- - - -	———			2,4
Bulimina strobila-farafraensis	0.77826	-0.34354	- - - -	———	———		1,4
Bulimina thanetensis	-0.6039	0.28786					
Cibicidoides alleni	-0.54094	0.31813			———		1
Cibicidoides cf. *C. hyphalus*	-0.40509	0.067504			———		1,3,4
Cibicidoides pseudoacutus	-0.40946	0.062275		———		- - - -	1-4
Cibicidoides rigidus	-0.41567	0.048179		———		- - - -	3,4
cf. *Cibicidoides sp. (epiphytic)*	-0.45703	-0.16408	- - -				*
Cibicidoides succedens	-0.59655	0.37592		———		- - - -	1,2,4
Coryphostoma cf. *C. midwayensis*	-0.56883	0.46301			———		1
Dentalina spp.	-0.37579	-0.21029					
Dorothia spp.	-0.69102	0.63812			———		2
Eponides lunatus	-0.57703	0.41027					
Gaudryina pyramidata	-0.43071	0.11259			———		1
Gaudryina spp.	-0.48724	0.12576			———		1
Gavelinella beccariiformis	-0.73636	0.78364				—	1
Globocasssidulina subglobosa	-0.51936	0.26557			———		1,3,4
Gyroidinoides globosus	-0.54741	0.26198				—	1
Gyroidinoides cf. *G. tellburmaensis*	-0.30047	-0.06803			—		2
Gyroidinoides sp. A	-0.43392	0.12887					
Gyroidinoides spp.	-0.037423	-0.4272	- - -	- - -	- - -		*
Hansenisca girardanus	-0.019626	-0.21564	- - - -	———		- - - -	1,2,4
lenticulinids costate	1.6773	0.33307	—				1,4
lenticulinids smooth	0.12866	-0.01172		———		- - - -	1,2,3
Loxostomoides applinae	-0.4731	-0.03284	- - - -	———		- - - -	1,2,4
Marginulina spp.	0.60592	0.10764		———			1,2
monothalamous taxa	0.30033	0.32546	—	- - -	- - -	- - -	*
Neoeponides duwi	2.0314	0.74305	———	———			1,2
nodosariids smooth	-0.11285	0.046512		———		- - - -	1,2
nodosariids costate	0.52851	-0.02109		—	- - - -		1
Inuttallides truempyi	-0.73745	0.76425				—	1
Oridorsalis plummerae	-0.27724	-0.07742		———		- - - -	1-4
Osangularia plummerae	-0.58675	0.45815		- - - -	———		1-4
Pullenia jarvisi group	-0.47658	0.26897			———		1
Pulsiphonina prima	-0.52561	0.18098			———		1,3
Quadrimorphina spp.	-0.40012	-0.12267			—	- - - -	2
Siphogenerinoides elegantus	-0.32863	0.091314		———		- - - -	1,2,4
Siphogenerinoides esnehensis	0.070741	-0.77917		—			1
Spiroloculina spp.	-0.32675	-0.21763		———			2
Spiroplectinella dentata	-0.3204	-0.07508			———		1,2
Spiroplectinella knebeli	-0.52623	0.2137		- - - -	———		1,2
Sporobulimina eocaena	-0.29999	-0.01984			———		1,3,4
Stainforthia / Uvigerinella spp.	0.46734	0.033389		———	———		1,2
Stilostomella spp.	0.81884	-1.895			———		1
Tappanina selmensis	0.022497	-0.37648		———		- - - -	2
Tritaxia midwayensis	-0.56384	0.31364			———		1,2
non-calcareous agglutinated taxa	1.0409	-0.04197	———	———			1,2,4
Valvalabamina depressa	-0.35454	-0.03446	- - - -	———		- - - -	1-4
Valvalabamina planulata	-0.26992	-0.18608	- - - -	- - - -	———		1,3,4
Valvulinreria (?) *insueta*	-0.59744	0.356	- - -	- - -	- - -		*

presence of (oxidized) pyrite, gypsum and/or anhydrite, and organic carbon enrichment.

Sprong et al. (2011) present geochemical analyses of the LDE in the Qreiya 3 section. Below the LDE, no evidence is found for high organic loading, and the redox-sensitive trace elements (U, Cu, As, Ni, Zn) show no enrichment, indicating normal marine, well-oxygenated bottom-water environments. At the base of the LDE the amount of organic matter (total organic carbon (TOC) up to 4%), as well as the concentrations of redox-sensitive trace elements increase abruptly and show peak values in the lower LDE bed I. This coincides with the abrupt

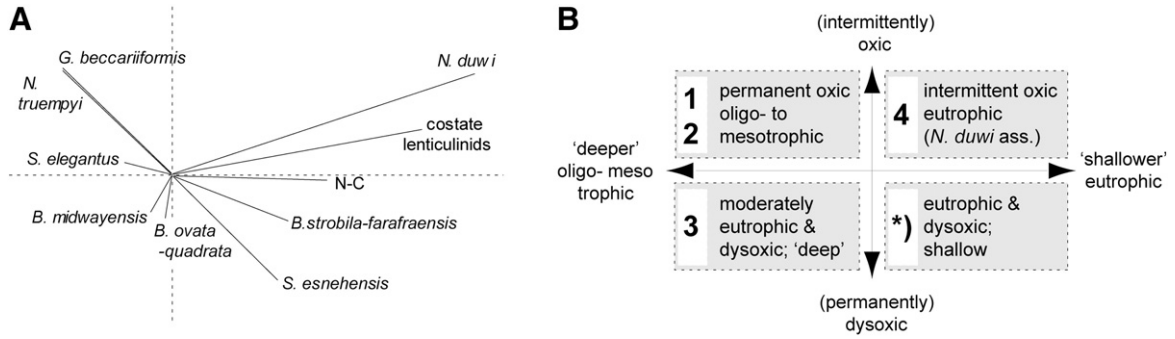

Fig. 7. R-mode correspondence analysis. Taxa in all sections were taken together. A: Distribution of important taxa in bivariate space. B: Interpretation of the first and second CA axes. Numbers 1–4 correspond to benthic foraminiferal assemblages distinguished by Q-mode CA (see Fig. 6). The field denoted by an asterisk represents conditions in which benthic foraminiferal faunas are greatly reduced or absent.

lithological change at the base of the LDE, and with changes in benthic foraminiferal distribution, which also point to dys- or anoxia. The TOC and the redox-sensitive trace elements return to background values in LDE bed II.

5.2.2. Benthic foraminifera

In LDE bed I the BFN are extremely low, at some levels near zero, and the diversity is at a minimum (Fig. 5A, B; Appendix A). In LDE bed I in the Qreiya 3 section, in-situ benthic foraminifera are absent. During the LDE all pre-LDE benthic assemblages are replaced by low-diversity assemblages dominated by a succession of few taxa: *Siphogenerinoides esnehensis*, buliminids, and *Neoeponides duwi*, together with, among others, costate lenticulinids (Fig. 5; Appendix A). After the LDE the same or similar assemblages as present before the LDE return in all sections. Eutrophication is indicated in the younger sediments of the longer sections by the increasing abundances of buliminids.

In the Q-mode correspondence analysis (CA), run on samples from each section separately, the LDE beds are represented by samples containing assemblage 4A (Fig. 6). This assemblage is included within the inner to middle neritic assemblage 4 in the shallower sections Aweina and Duwi. It is separated in the deeper Qreiya 1 and 3 and Araas sections, probably because it deviates more from the outer neritic to bathyal assemblages present in the deeper sections before and after the LDE.

The Q-mode CA reflects an environmental gradient between an outer-neritic to bathyal, meso- to oligotrophic end member present before and after the LDE, and an inner to middle neritic, eutrophic end member dominating during the LDE. Assemblages 1 (outer neritic to bathyal: Araas and Qreiya 1 and 3 sections), and 2 (middle to

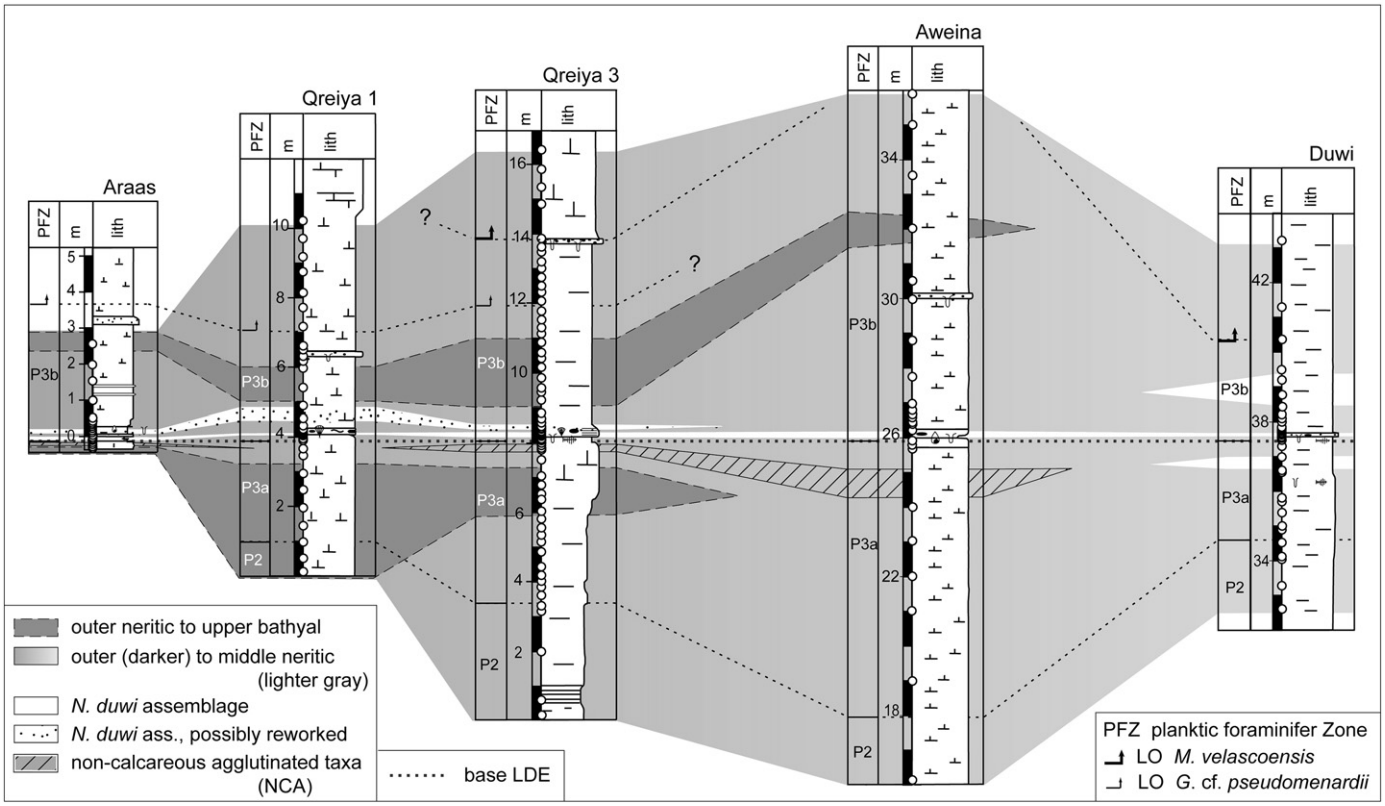

Fig. 8. Fence diagram of the five studied sections. The sections are arranged according to paleodepth, with the deepest, outer neritic to bathyal sections to the left (Araas, Qreiya 1 and Qreiya 3) and the shallowest, middle neritic section to the right (Duwi). Dissolution levels (hatched) occur in the Araas, Qreiya 3 and Aweina sections below the LDE. Incursions of the *N. duwi* assemblage (white) occur in all sections during the LDE. Three incursions of *N. duwi* are recorded in the Duwi section. In the Qreiya 1, Qreiya 3 and Araas sections the younger incursion of *N. duwi* must perhaps be attributed to reworking (stippled).

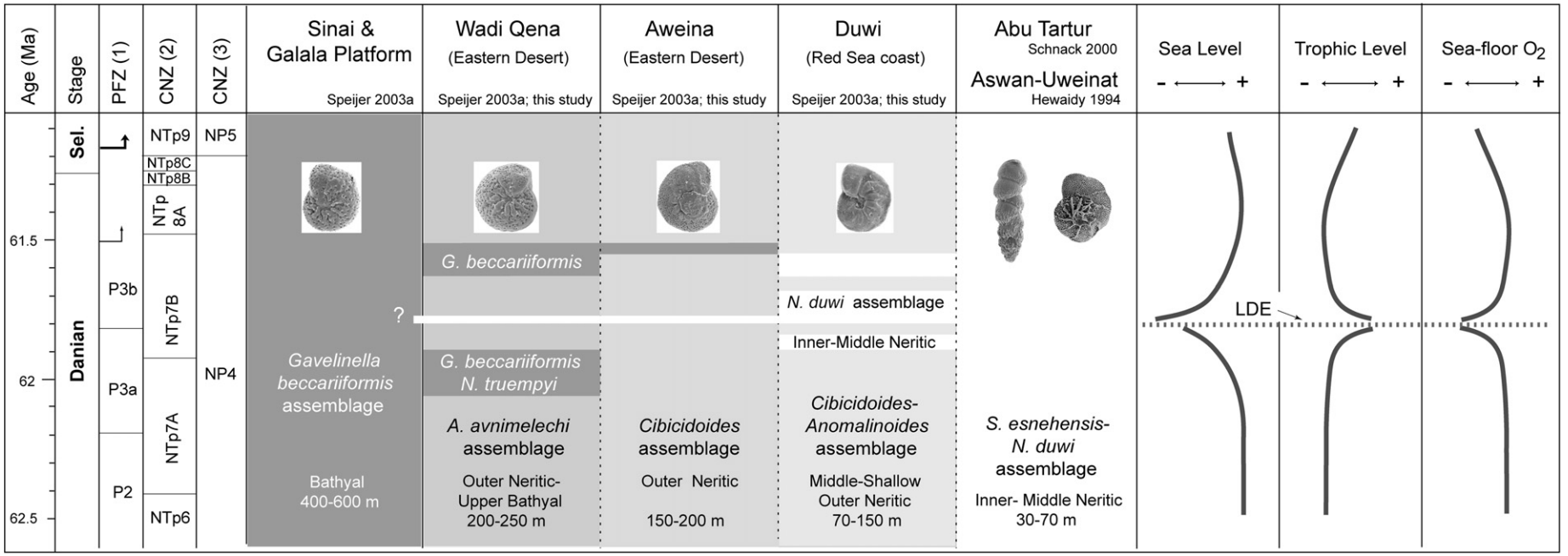

Fig. 9. Graphic summary of the studied bathymetric transect across the LDE. Sinai and Galala Platform (left) taken from Speijer (2003a). Abu Tartur taken from Schnack (2000). Aswan-Uweinat taken from Hewaidy (1994). All other locations adapted from Speijer (2003a) based on results of this study. *Neoeponides duwi* has not been recorded in the Galala Platform, but is a common species in the shallow Abu Tartur and Aswan-Uweinat Basins. White bars represent incursions of the *N. duwi* assemblage. To the right: schematic representation of bottom-water environment in the sections studied. Dashed gray line represents the base of the LDE. Shallowing across the LDE is associated with oxygen depletion and eutrophication, reflected in the lithology and the benthic foraminiferal assemblages.

outer neritic, Aweina and Duwi sections) represent background conditions in the Dakhla Fm.

Similarly, the R-mode CA on species of all sections (Fig. 7A) primarily separates deeper-water, oligotrophic taxa (*G. beccariiformis*; *N. truempyi*: e.g., Thomas, 1998) from shallower-water, eutrophic taxa such as the buliminids. The buliminids, commonly associated with eutrophic, oxygen-poor environments (e.g., Corliss and Chen, 1988; Jorissen et al., 1995) are positioned on the negative side of the second axis. The assemblages 1–4 and 4A, distinguished in the Q-mode CA (Fig. 6), are also distinguished in the fields defined by the axes of the R-mode CA (Fig. 7B). In this interpretation, *N. duwi* is a taxon capable of living in relatively shallow, eutrophic environments characterized by periods of dysoxia. The field denoted by an asterisk (lower right in Fig. 7B) represents the conditions at the base of the LDE, where in-situ benthic foraminiferal faunas are either absent, or greatly reduced.

5.3. Assessment of paleobathymetry

5.3.1. Reliability of P/B ratios

Despite the differences in depositional depths (Fig. 2; Section 4.2.1), the P/B ratios are in a similar range in all sections (between 70 and 90–95% planktics below and above the LDE) and thus do not accurately resolve differences in paleodepth between the sections in the depth transect. In addition, based on P/B ratios alone, the apparent shallowing at the base of the LDE beds is greatly overestimated. An estimate of paleodepth based on P/B ratios is most reliable in relatively stable, open marine environments (e.g., Van der Zwaan et al., 1990). Environmental parameters at the sea floor (oxygenation; organic load) can strongly affect the ratio between planktic and benthic foraminifera in unpredictable ways. Excessive supply of organic matter may lead to increased benthic numbers and lower P/B ratios, and might also result in low diversity, because resilient taxa are blooming, and more specialized taxa disappear. However, if the oxidation of excessive organic load depletes oxygen, and if oxygen depletion is sustained for a longer period, conditions may become too adverse for foraminifera. This may lead to an overestimation of paleodepth due to reduced benthic, and relatively high planktic numbers, such as observed at some levels in LDE bed I.

In addition, weathering and diagenesis must be considered. Dissolution will affect the most fragile foraminiferal tests first: often in a particular sequence from fragile planktics to robust benthics (e.g., Nguyen et al., 2009 and references therein). Since dissolution may be a consequence of pore water acidification due to excessive organic decay and pyrite oxidation, the two parameters are not easily untangled, and paleodepth reconstructions based on P/B ratios can be seriously flawed.

Finally, evidence exists that some benthic foraminifera are able to shift from one depth domain to another pursuing favorable conditions, such as prolific food supply (Pflum and Frerichs, 1976; Speijer et al., 1997). Paleodepth reconstructions attempted at the PETM and based on P/B ratios have proven equally problematic (e.g., Speijer et al., 1997; Speijer, 2003a).

To summarize, we suggest that the paleoenvironmental conditions during the LDE, with evidence for anoxia and for post-depositional alteration, strongly limit the use of P/B ratios to reconstruct paleodepth. Consequently, we mostly rely on well-documented depth distributions of benthic foraminiferal assemblages – preferably not of individual species – derived from literature and own observations. Although the numeric depth estimates in the five sections have fairly large uncertainties, we are confident that, based on regional biofacies distributions, the depth difference between the deepest (Qreiya 1 and 3, Araas) and shallowest (Duwi) sections is at least 100 m.

5.3.2. The Neoeponides duwi assemblage

Schnack (2000) documented *N. duwi* (as *Discorbis duwiensis*) in assemblages from the shallow Abu Tartur Plateau in Zones P1–P3b, often occurring in large numbers in short-lived pulses. Speijer (2003b) found abundant *N. duwi* occurring in TOC-enriched sediments around the Danian/Selandian transition, the interval now considered as the LDE. The incursion of *N. duwi* in LDE bed II at Qreiya 3 was interpreted by Sprong et al. (2011) as depth migration of a species into an environment that was vacated by benthic foraminifera due to anoxia in LDE bed I.

A consequence of depth migration of a species is, that it is not a reliable paleodepth indicator. However, taxa associated with abundant *N. duwi* may provide a paleodepth estimate. Where *N. duwi* is extremely dominant, associated taxa are commonly *Siphogenerinoides esnehensis* together with lenticulinids and buliminids. Probably *S. esnehensis* is a species occurring in middle to outer neritic environments. It was reported from the late Cretaceous and Paleocene of the Duwi section (Nakkady, 1950; Anan, 1998, as *Orthokarstenia higazyi*), and in sections in the Kharga Oasis (Anan and Sharabi, 1988, also as *O. higazyi*) together with, among others, *Alabamina midwayensis*, *Hansenisca* (*Gyroidinoides*) *girardanus*, and *Loxostomoides applinae*. This is in agreement with the co-occurrence of *N. duwi* and *S. esnehensis* with middle to outer neritic taxa such as *Alabamina midwayensis*, *Anomalinoides midwayensis*, and *B. strobila* in our material.

Where *N. duwi* is less dominant, NCA taxa, including *Haplophragmoides* spp. occur in the assemblage. The association with relatively abundant agglutinated taxa and lenticulinids indicates that *N. duwi* is to a certain extent dissolution-resistant, which is in agreement with its robust morphology. This also suggests that *N. duwi* thrives in specific, food-rich and oxygen-depleted environments in a broad range of paleodepths. Consequently, the *N. duwi* assemblage probably does not reflect shallowing to inner neritic depths, but more likely indicates disturbed conditions at inner- to outer neritic depths, associated with high organic load, and (intermittent) dys- or anoxic conditions at the sea floor. Speijer (2003b) proposed that *N. duwi* even had the ability to rapidly repopulate an anoxic seafloor during transient oxygenation events, an adaptation very similar to *Anomalinoides aegyptiacus* during the PETM in Egypt (Speijer et al., 1997). This interpretation, however, was based on the assumption that the rare specimens of *N. duwi* in the basal laminated part of LDE bed I were in situ. Our detailed sampling and careful removal of bioturbations from this bed at Qreiya 3 reveals that this assumption is not valid.

5.3.3. Timing and magnitude of pre-LDE shallowing

Shallowing preceding the LDE was estimated to be 50 m or less in the Qreiya 3 section (Sprong et al., 2011). This estimate was based on the disappearance of the bathyal species (mainly *G. beccariiformis* and *N. truempyi*) well before the onset of the LDE, and persistence of a diverse assemblage composed of outer neritic taxa such as *Cibicidoides* spp. and *Osangularia plummerae* until the onset of the LDE. Bias by dissolution, dysoxia or eutrophication could be excluded.

In the depth transect studied here, pre-LDE shallowing can be evaluated in the deeper sections Qreiya 1 and 3 and Araas (Fig. 5A, B; Appendix A). Bathyal species (*G. beccariiformis*, *N. truempyi*) disappear well before the LDE, whereas the *N. duwi* assemblage, indicating disturbed sea-floor environments (Section 5.3.2), is not yet dominant. In the Qreiya 1 and 3 sections a diverse, outer neritic assemblage persists up to the base of LDE bed I. The absence of bathyal taxa before the LDE is probably not caused by adverse environmental conditions, such as eutrophication or dysoxia, but by shallowing from deep outer neritic-upper bathyal to outer neritic depths and may have amounted to 50 m or less, in agreement with Sprong et al. (2011). In the Araas section the pattern below the LDE is less clear, but here reworking cannot be excluded.

Earlier estimates of shallowing exceeding 100 m associated with the LDE at Aweina (Speijer and Schmitz, 1998) seem unlikely. Shallowing of 100 m or more should be readily visible in marked erosional

features of the Duwi section, being the shallowest in the depth transect (~70–150 m). Such features are not observed.

5.4. Summary of the LDE in the transect

The five sections discussed in this report are positioned along a paleobathymetric transect ranging between 70–150 (Duwi) and 150–250 m (the Araas and Qreiya sections; Fig. 8). Prominent dissolution intervals below the LDE occur in the Araas, Qreiya 3 and Aweina sections. A relative sea-level fall before the LDE, and subsequent rise was proposed for the Aweina section (Speijer and Schmitz, 1998; Speijer, 2003a). Sprong et al. (2011) provide arguments for a sea-level fall of ~50 m or less at Qreiya 3 before the LDE, and explain anoxia during deposition of LDE bed I by rapid sea-level rise, assigned to a transgressive systems tract. The base of the LDE is considered a sequence boundary without evidence for sea-level lowstand deposits.

The data in the present report support this interpretation (Fig. 9). A sharp lithologic boundary occurs between the base of the LDE and the underlying strata, and in all sections except Duwi, indications for oxygen depletion are seen in the lower LDE Bed I. These observations are also typical for PETM sequences on the Egyptian shelf (e.g., Speijer and Wagner, 2002), and fit the model for transgressive black shales developed for Jurassic deposits (e.g., Wignall and Newton, 2001). The estimated magnitude of the sea-level cycle associated with the LDE (≤50 m) may exceed estimates for the PETM (20–30 m: e.g., Speijer and Morsi, 2002; Sluijs et al., 2008), but a lower limit to sea-level change is difficult to constrain in the sections in the Nile Basin.

During deposition of LDE bed II, oxygen was intermittently available at the sea floor, favoring the occurrence of a *N. duwi* assemblage including buliminids and *S. esnehensis*. Eventually, *N. duwi* disappeared, whereas buliminids and *S. esnehensis* lingered on until normal marine, pre-LDE conditions were restored.

Repeated incursions of *N. duwi* occur in all sections except Aweina, amounting to three in the Duwi section (Figs. 5a, b, 8; Appendix A). Influxes not associated with LDE Bed II but higher up-section, occurring in the Duwi section (see also Speijer, 2003a) are probably caused by the fact that the Duwi section is relatively shallow, and eutrophication sets in shortly after the LDE. In the Araas section, downward bioturbation of the *N. duwi* assemblage cannot be excluded. On a regional scale (Fig. 9) it appears that the normal distribution of *N. duwi* is limited to inner and middle neritic environments, like at Abu Tartur and Aswan (e.g., Schnack, 2000), and the incursions at deeper locations represent disturbed bottom-water environments during the LDE.

5.5. Comparison with other proposed Paleocene transient warming episodes

The LDE correlates with the CIE-DS1 at Zumaia and the Top Chron C27n event in the Atlantic and Pacific Oceans (Bornemann et al., 2009; Westerhold et al., 2011). At ODP Site 1209 the LDE is associated with a benthic $\delta^{13}C$ excursion of 0.6‰ and a deep-water temperature increase of 2 °C, suggesting that the LDE is a global transient warming episode. It is therefore remarkable that the rather severe perturbations of the benthic foraminiferal assemblages such as seen across the LDE in this study were absent during the CIE-DS1 in the Zumaia section, where only a shift in the infaunal/epifaunal ratio of the benthic foraminifera was found (Arenillas et al., 2008). This different expression may perhaps be attributed to the greater depositional depth of the Zumaia section (estimated at 900–1100 m).

Other proposed Paleocene hyperthermals are the Dan-C2 event (~65.2 Ma) and the ELPE or MPBE (~58.9 Ma) (Westerhold et al., 2011). The Dan-C2 event in the NW and SE Atlantic (ODP Hole 1049C; DSDP Holes 527 and 528: Quillévéré et al., 2002, 2008) are characterized by two, relatively short-lived (~40 kyr), moderate (~1–1.5‰) shifts towards lighter $\delta^{13}C$ and $\delta^{18}O$. Together with the duration of the event, estimated at ~100 kyr, this suggests orbital control (Quillévéré et al., 2008). Coccioni et al. (2010) described the Dan-C2 event in the land-based Contessa Highway section in Italy, where the double shifts in $\delta^{13}C$ and $\delta^{18}O$ were also found. Disturbance of the benthic assemblages was reported, including indications for low sea-floor oxygen levels, and increased organic carbon flux.

The Early Late Paleocene Event (ELPE, ODP Leg 198, Shatsky Rise: Bralower et al., 2002, 2006; Petrizzo, 2005) or Mid-Paleocene Biotic Event (MPBE, Zumaia: Bernaola et al., 2007) occurred around 58.5 Ma (Westerhold et al., 2011). At Site 1209 (Shatsky Rise) an isotope shift associated with the ELPE could not be resolved due to condensation and carbonate dissolution (Westerhold et al., 2011). In the Zumaia section Bernaola et al. (2007) estimated the duration of the event at ~52–53 kyr. A negative $\delta^{13}C$ shift, with an estimated duration of 10–11 kyr, amounted to ~1‰ in bulk sediment. The MPBE at Zumaia affected sea surface as well as sea floor biota. The benthic assemblage composition changed considerably, and agglutinated benthic foraminifera increased in abundance, associated with decreased calcium carbonate levels, suggestive of dissolution phenomena (Nguyen et al., 2009).

Each of the three events shares characteristics with the PETM, such as lithologic change and a (moderate) CIE, although the ELPE is not yet fully resolved. More or less severe perturbations of the benthic environment are seen during each of the events, and are associated with carbonate dissolution, oxygen depletion at the sea floor and increased organic flux. However, sea-level fluctuations, which are also a characteristic feature of the PETM (e.g., Speijer and Morsi, 2002; Ernst et al., 2006; Sluijs et al., 2008) have until now only been reported from the LDE on the southern Tethyan shelf. In addition, by correlation with the Zumaia section Bornemann et al. (2009) estimated the duration of the LDE to be ~190 kyr. Based on high-resolution chronology in Site 1209, Westerhold et al. (2011) calculated a similar duration of ~200 kyr for the Top Chron C27n (=LDE) event. This is similar to the estimated duration of the PETM in Röhl et al. (2000, 2007), and exceeds estimates for the Dan-C2 and ELPE/MPBE.

6. Conclusions

The five sections included in this study represent a paleobathymetric transect ranging between middle to outer neritic, and deep outer-neritic to upper-bathyal depths. Along this transect all sections except the Duwi section show a similar lithologic sequence across the LDE, including a lower LDE bed I with levels (nearly) barren of benthic foraminifera, and an incursion of a *N. duwi* assemblage in upper LDE bed II. During the onset of the LDE widespread, short-lived sea-floor dysoxia during rapid transgression prevailed in the deeper parts of the basin.

Based on the depth distribution of benthic foraminiferal assemblages, shallowing preceding, and deepening associated with the LDE are estimated to be about 50 m or less. This would exceed the estimate for the PETM, which is about 20–30 m. The P/B ratio (%P) is of limited use in assessing the sea-level history of the LDE, as it is affected by parameters other than depositional depth, such as oxygen depletion, eutrophication and dissolution.

The correlation of the CIE associated with the LDE in the Nile Basin with isotope records in major oceanic basins suggests that the LDE is the expression of a transient warming episode on the southern Tethyan margin, similar to other proposed transient warming events, such as the Dan-C2 event and the MPBE/ELPE. The LDE as documented here may differ from these events in the evidence for a sea-level cycle associated with the LDE, and the duration of the LDE, which exceeds the estimated duration of both the Dan-C2 and the MPBE/ELPE.

Supplementary materials related to this article can be found online at doi:10.1016/j.marmicro.2012.01.001.

Acknowledgements

We thank Birger Schmitz for using samples collected in 1995 at Gebel Aweina. Thoughtful reviews by Frédéric Quillévéré and two anonymous reviewers are greatly appreciated and helped improving the manuscript. This study was supported by grants from the Research Foundation – Flanders (FWO – G.0527.05), the K.U. Leuven Research Fund, and the Herta and Hartmut Schmauser Stiftung from the University of Erlangen.

References

Agnini, C., Macrì, P., Backman, J., Brinkhuis, H., Fornaciari, E., Giusberti, L., Luciani, V., Rio, D., Sluijs, A., Speranza, F., 2009. An early Eocene carbon cycle perturbation at 52.5 Ma in the Southern Alps: Chronology and biotic response. Paleoceanography 24. doi:10.1029/2008PA001649.

Al Rifaiy, I.A., Cherif, O.H., 1987. Biostratigraphic aspects and regional correlation of some Cenomanian/Turonian exposures in Jordan. Géologie Mediterranéenne XIV, 181–193.

Anan, H.S., 1998. Accelerated evolution in representatives of the genera *Orthokarstenia* and *Discorbis* (benthic foraminifera) in the Maastrichtian and Paleocene of Egypt (Misr). Neues Jahrbuch für Geologie und Paläontoogie, Monatshefte 6, 365–375.

Anan, H.S., Sharabi, S.A., 1988. Benthonic foraminifera from the Upper Cretaceous-Lower Tertiary rocks of the northwest Kharga Oasis, Egypt. M.E.R.C. Ain Shams University. Earth Sciences Series 2, 191–218.

Arenillas, I., Molina, E., Ortiz, S., Schmitz, B., 2008. Foraminiferal and stable isotopic event-stratigraphy across the Danian−Selandian transition at Zumaya (northern Spain): chronostratigraphic implications. Terra Nova 20, 38–44.

Bartov, Y., Steinitz, G., 1977. The Judea and Mount Scopus Groups in the Negev and Sinai with trend surface analysis of the thickness data. Israel Journal of Earth Sciences 26, 119–148.

Bauer, J., Kuss, J., Steuber, T., 2003. Sequence architecture and carbonate platform configuration (upper Cenomanian-Santonian), Sinai, Egypt. Sedimentology 50, 387–414.

Berger, W.H., Diester-Haass, L., 1988. Paleoproductivity; the benthic/planktonic ratio in foraminifera as a productivity index. Marine Geology 81, 15–25.

Berggren, W.A., Pearson, P.N., 2005. A revised tropical to subtropical Paleogene planktonic foraminiferal zonation. Journal of Foraminiferal Research 35, 279–314.

Bernaola, G., Baceta, J.I., Orue-Etxebarria, X., Alegret, L., Martín-Rubio, M., Arostegui, J., Dinarès-Turell, J., 2007. Evidence of an abrupt environmental disruption during the mid-Paleocene biotic event (Zumaia section, western Pyrenees). GSA Bulletin 119. doi:10.1130/B26132.1.

Bornemann, A., Schulte, P., Sprong, J., Steurbaut, E., Youssef, M., Speijer, R.P., 2009. Latest Danian carbon isotope anomaly and associated environmental change in the southern Tethys (Nile Basin, Egypt). Journal of the Geological Society of London 166, 1135–1142. doi:10.1144/0016-76492008-104.

Bralower, T.J., Premoli Silva, I., Malone, M.J., and 24 others, 2002. Proceedings of the Ocean Drilling Program, Initial reports, Leg 198. http://www-odp.tamu.edu/publications/198_IR/198ir.htm2002.

Bralower, T.J., Premoli-Silva, I., Malone, M.J., 2006. Leg 198 Synthesis: a remarkable 120-M.Y. record of climate and oceanography from Shatsky Rise, Northwest Pacific Ocean. In: Bralower, T.J., Premoli Silva, I., Malone, M.J. (Eds.), Proceedings of the Ocean Drilling Program: Scientific Results, 198, pp. 1–47. College Station, TX.

Coccioni, R., Frontalini, F., Bancalà, G., Fornaciari, E., Jovane, L., Sprovieri, M., 2010. The Dan-C2 hyperthermal event at Gubbio (Italy): global implications, environmental effects, and cause(s). Earth and Planetary Science Letters 297, 298–305.

Corliss, B.H., Chen, C., 1988. Morphotype patterns of Norwegian Sea deep-sea benthic foraminifera and ecological implications. Geology 16, 716–719.

Cramer, B.S., Wright, J.D., Kent, D.V., Aubry, M.-P., 2003. Orbital climate forcing of δ13C excursions in the late Paleocene–early Eocene (chrons C24n–C25n). Paleoceanography 18. doi:10.1029/2003PA000909.

Dickens, G.R., Castillo, M.M., Walker, J.C.G., 1997. A blast of gas in the latest Paleocene; simulating first-order effects of massive dissociation of oceanic methane hydrate. Geology 25, 259–262.

Dinarès-Turell, J., Baceta, J.I., Pujalte, V., Orue-Etxebarria, X., Bernaola, G., Lorito, S., 2003. Untangling the Paleocene climate rhythm: an astronomically calibrated Early Paleocene magnetostratigraphy and biostratigraphy at Zumaia (Basque Basin, northern Spain). Earth and Planetary Science Letters 216, 483–500.

Dinarès-Turell, J., Stoykova, K., Baceta, J.I., Ivanov, M., Pujalte, V., 2010. High-resolution intra- and interbasinal correlation of the Danian–Selandian transition (Early Paleocene): the Bjala section (Bulgaria) and the Selandian GSSP at Zumaia (Spain). Palaeogeography, Palaeoclimatology, Palaeoecology 297, 511–533.

Ernst, S.R., Guasti, E., Dupuis, C., Speijer, R.P., 2006. Environmental perturbation in the southern Tethys across the Paleocene/Eocene boundary (Dababiya, Egypt): foraminiferal and clay mineral records. Marine Micropaleontology 60, 89–111.

Guiraud, R., Bosworth, W., 1999. Phanerozoic geodynamic evolution of northeastern Africa and the northwestern Arabian platform. Tectonophysics 315, 73–108.

Hammer, Ø., Harper, D.A.T., Ryan, P.D., 2001. PAST: Paleontological Statistics: Software Package for Education and Data Analysis. Palaeontologia Electronica 4 http://palaeo-electronica.org/2001_1/past/issue1_01.htm.

Hendriks, F., Luger, P., Bowitz, J., Kallenbach, H., 1987. Evolution of depositional environments of SE Egypt during the Cretaceous and lower Tertiary. Berliner Geowissenschaftliche Abhandlungen, (A): Geologie und Paläontologie 75, 49–82.

Hewaidy, A.G.A., 1994. Biostratigraphy and paleobathymetry of the Garra-Kurkur area, southwest Aswan, Egypt. Middle East Research Center Ain Shams University. Earth Science Series 8, 48–73.

Higgins, J.A., Schrag, D.P., 2006. Beyond methane: towards a theory for the Paleocene–Eocene thermal maximum. Earth and Planetary Science Letters 245, 523–537.

Higgs, N.C., Thomson, J., Wilson, T.R.S., Croudace, I.W., 1994. Modification and complete removal of eastern Mediterranean sapropels by postdepositional oxidation. Geology 22, 423–426.

Jorissen, F.J., De Stigter, H.C., Widmark, J.G.V., 1995. A conceptual model explaining benthic foraminifera microhabitats. In: Langer, M.R. (Ed.), FORAMS 1994: Marine Micropaleontology, 26, pp. 3–15.

Kennett, J.P., Stott, L.D., 1991. Abrupt deep-sea warming, palaeoceanographic changes and benthic extinctions at the end of the Palaeocene. Nature 353, 225–229.

Kent, D.V., Cramer, B.S., Lanci, L., Wang, D., Wright, J.D., Van Der Voo, R., 2003. A case for a comet impact trigger for the Paleocene/Eocene thermal maximum and carbon isotope excursion. Earth and Planetary Science Letters 211, 13–26.

Kuhnt, W., Moullade, M., Kaminski, M.A., 1996. Ecological structuring and evolution of deep sea agglutinated foraminifera — a review. Revue de Micropaleontologie 39, 271–281.

Lourens, L.J., Sluijs, A., Kroon, D., Zachos, J.C., Thomas, E., Röhl, U., Bowles, J., Raffi, I., 2005. Astronomical pacing of late Palaeocene to early Eocene global warming events. Nature 435, 1083–1087.

Luger, P., 1985. Stratigraphie der marinen Oberkreide und des Alttertiärs im südwestlichen Obernil-Becken (SW Ägypten) unter besonderer Berücksichtigung der Mikropaläontologie, Palökologie und Paläogeographie. Berliner Geowissenschaftliche Abhandlungen, Reihe A: Geologie und Paläontologie 63, 151.

Luger, P., 1988. Maestrichtian to Paleocene facies evolution and Cretaceous/Tertiary boundary in middle and southern Egypt. Revista Espanola de Paleontologia 83–90 Numero extraordinario.

Lunt, D.J., Ridgwell, A., Sluijs, A., Zachos, J., Hunter, S., Haywood, A., 2011. A model for orbital pacing of methane hydrate destabilization during the Palaeogene. Nature Geosciences. doi:10.1038/NGEO1266 Advance Online Publication 2 October 2011.

Luterbacher, H.P., Ali, J.R., Brinkhuis, H., et al., 2004. The Paleogene period. In: Gradstein, F.M., Ogg, J.G., Smith, A.G. (Eds.), A Geologic Time Scale 2004. Cambridge University Press. 610 pp.

Mart, Y., 1991. Some Cretaceous and early Tertiary structures along the distal continental margin of the southeastern Mediterranean. Israel Journal of Earth Sciences 40, 77–90.

Martini, E., 1971. Standard Tertiary and Quaternary calcareous nannoplankton zonation. In: Farinacci, A. (Ed.), Proceedings of the 2nd Planktonic Conference, Rome, 1970: Tecnoscienza, pp. 739–785. Rome.

Nakkady, S.E., 1950. A new foraminiferal fauna from the Esna shales and upper Cretaceous chalk of Egypt. Journal of Paleontology 24, 688.

Nguyen, T.M.P., Petrizzo, M.R., Speijer, R.P., 2009. Experimental dissolution of a fossil foraminiferal assemblage (Paleocene–Eocene Thermal Maximum, Dababiya, Egypt): Implications for paleoenvironmental reconstructions. Marine Micropaleontology 73, 241–258.

Nicolo, M.J., Dickens, G.R., Hollis, C.J., Zachos, J.C., 2007. Multiple early Eocene hyperthermals: their sedimentary expression on the New Zealand continental margin and in the deep sea. Geology 35, 699–702.

Norris, R.D., Röhl, U., 1999. Carbon cycling and chronology of climate warming during the Palaeocene/Eocene transition. Nature 401, 775–778.

Olsson, R.K., Hemleben, C., Berggren, W.A., Huber, B.T. (Eds.), 1999. Atlas of Paleocene planktonic foraminifera: Smithsonian contributions to Paleobiology, 85, pp. 1–254.

Petrizzo, M.R., 2005. An early late Paleocene event on Shatsky Rise, northwest Pacific Ocean (ODP Leg 198): Evidence from planktonic foraminiferal assemblages. In: Bralower, T.J., Premoli Silva, I., Malone, M.J. (Eds.), An early late Paleocene event on Shatsky Rise, northwest Pacific Ocean (ODP Leg 198): Evidence from planktonic foraminiferal assemblages: Proceedings of the Ocean Drilling Project, Scientific Results, 198, pp. 1–29. College Station, Texas.

Pflum, C.E., Frerichs, W.E., 1976. Gulf of Mexico deep-water foraminifers: Cushman Foundation for Foraminiferal Research, Special Publication, 14, pp. 1–108.

Quillévéré, F., Norris, R.D., 2003. Ecological development of acarininids (planktonic foraminifera) and hydrographic evolution of Paleocene surface waters. In: Wing, S.L., Gingerich, P.D., Schmitz, B., Thomas, E. (Eds.), Causes and Consequences of globally warm climates in the Early Paleogene: Geological Society of America, Special Papers, 369, pp. 223–238.

Quillévéré, F., Aubry, M.-P., Norris, R.D., Berggren, W.A., 2002. Paleocene oceanography of the eastern subtropical Indian Ocean – an integrated magnetobiostratigraphic and stable isotope study of ODP Hole 761B (Wombat Plateau). Palaeogeography, Palaeoclimatology, Palaeoecology 184, 371–405.

Quillévéré, F., Norris, R.D., Kroon, D., Wilson, P.A., 2008. Transient ocean warming and shifts in carbon reservoirs during the early Danian. Earth and Planetary Science Letters 265, 600–615.

Röhl, U., Bralower, T.J., Norris, R.D., Wefer, G., 2000. New chronology for the late Paleocene thermal maximum and its environmental implications. Geology 28, 927–930.

Röhl, U., Westerhold, T., Bralower, T.J., Zachos, J.C., 2007. On the duration of the Paleocene–Eocene thermal maximum (PETM). Geochemistry, Geophysics, Geosystems 8, Q12002. doi:10.1029/2007GC001784.

Said, R., 1962. The geology of Egypt. Elsevier, Amsterdam, pp. 1–377.

Said, R., 1990. Cenozoic. In: Said, R. (Ed.), The geology of Egypt. A. A. Balkema, Brookfield, Rotterdam, pp. 451–486.

Scheibner, C., Reijmer, J.J.G., Marzouk, A.M., Speijer, R.P., Kuss, J., 2003. From platform to basin: the evolution of a Paleocene carbonate margin (Eastern Desert, Egypt).

International Journal of Earth Sciences 92, 624–640. doi:10.1007/s00531-003-0330-2.
Schmitz, B., Asaro, F., Molina, E., Monechi, S., von Salis, K., Speijer, R.P., 1997. High-resolution iridium, $\delta^{13}C$, $\delta^{18}O$, foraminifera and nannofossil profiles across the latest Paleocene benthic extinction event at Zumaya, Spain. Palaeogeography, Palaeoclimatology, Palaeoecology 133, 49–68.
Schmitz, B., Molina, E., Von Salis, K., 1998. The Zumaya section in Spain: a possible global stratotype section for the Selandian and Thanetian stages. Newsletters on Stratigraphy 36, 35–42.
Schnack, K., 2000. Biostratigraphie und fazielle Entwicklung in der Oberkreide und im Alttertiär im Bereich der Kharga Schwelle, Westliche Wüste, southwest Ägypten. Ph.D. Thesis Nr. 151, Universität Bremen, Bremen, 142 pp.
Shahar, J., 1994. The Syrian arc system: an overview. Palaeogeography, Palaeoclimatology, Palaeoecology 112, 125–142.
Shannon, C.E., Weaver, W., 1949. The Mathematical Theory of Communication. University of Illinois Press, Urbana. 117 pp.
Sluijs, A., Brinkhuis, H., Schouten, S., Bohaty, S.M., John, C.M., Zachos, J.C., Reichart, G.J., Sinninghe Damsté, J.S., Crouch, E.M., Dickens, G.R., 2007. Environmental precursors to rapid light carbon injection at the Palaeocene/Eocene boundary. Nature 450, 1218–1221.
Sluijs, A., Brinkhuis, H., Crouch, E.M., John, C.M., Handley, L., Munsterman, D., Bohaty, S., Zachos, J.C., Reichart, G.-J., Schouten, S., Pancost, R.D., Sinninghe Damsté, J.S., Welters, N.L.D., Lotter, A.F., Dickens, G.R., 2008. Eustatic variations during the Paleocene–Eocene greenhouse world. Paleoceanography 23, PA4216. doi:10.1029/2008PA001615.
Soliman, M.F., Obaidalla, N.A., 2010. Danian–Selandian transition at Gabal el-Qreiya section, Nile Valley (Egypt): lithostratigraphy, biostratigraphy, mineralogy and geochemistry. Neues Jahrbuch für Geologie und Paläontologie 258, 1–30.
Speijer, R.P., 2000. The late Paleocene event and a potential precursor compared: first results from Egypt. GFF 122, 150–151.
Speijer, R.P., 2003a. Systematics and paleoecology of the foraminifer *Neoeponides duwi* (Nakkady) from the Paleocene of Egypt. Micropaleontology 49, 146–150.
Speijer, R.P., 2003b. Danian–Selandian sea-level change and biotic excursion on the southern Tethyan margin. In: Wing, S.L., Gingerich, P.D., Schmitz, B., Thomas, E. (Eds.), Causes and consequences of globally warm climates in the Early Paleogene: Geological Society of America Special Paper, 369, pp. 275–290.
Speijer, R.P., Morsi, A.A.M., 2002. Ostracode turnover and sea-level changes associated with the Paleocene–Eocene thermal maximum. Geology 30, 23–26.
Speijer, R.P., Schmitz, B., 1998. A benthic foraminiferal record of Paleocene sea level and trophic/redox conditions at Gebel Aweina, Egypt. Palaeogeography, Palaeoclimatology, Palaeoecology 137, 79–101.
Speijer, R.P., Wagner, T., 2002. Sea-level changes and black shales associated with the late Paleocene thermal maximum (LPTM); organic-geochemical and micropaleontologic evidence from the southern Tethyan margin (Egypt-Israel). In: Koeberl, C., MacLeod, K.G. (Eds.), Catastrophic Events and Mass Extinctions: Impacts and Beyond: Geological Society of America Special Paper, 356, pp. 533–549.
Speijer, R.P., Schmitz, B., Van der Zwaan, G.J., 1997. Benthic foraminiferal extinction and repopulation in response to latest Paleocene Tethyan anoxia. Geology 25, 683–686.
Spellerberg, I.F., Fedor, P.J., 2003. A tribute to Claude Shannon (1916–2001) and a plea for more rigorous use of species richness, species diversity and the 'Shannon–Wiener' Index. Global Ecology and Biogeography 12, 177–179.
Sprong, J., Speijer, R.P., Steurbaut, E., 2009. Biostratigraphy of the Danian/Selandian transition in the southern Tethys, with special reference to the Lowest Occurrence of planktic foraminifera *Igorina albeari*. Geologica Acta 7, 63–77.
Sprong, J., Youssef, M.A., Bornemann, A., Schulte, P., Steurbaut, E., Stassen, P., Kouwenhoven, T.J., Speijer, R.P., 2011. A multi-proxy record of the Latest Danian Event at Gebel Qreiya, Eastern Desert, Egypt. Journal of Micropalaeontology 30, 167–182.
Stap, L., Sluijs, A., Thomas, E., Lourens, L., 2009. Patterns and magnitude of deep sea carbonate dissolution during Eocene Thermal Maximum 2 and H2, Walvis Ridge, southeastern Atlantic Ocean. Paleoceanography 24 (PA1211). doi:10.1029/2008PA001655 13 pp.
Stassen, P., Dupuis, C., Morsi, A.M., Steurbaut, E., Speijer, R.P., 2009. Reconstruction of a latest Paleocene shallow-marine eutrophic paleoenvironment at Sidi Nasseur (Central Tunisia) based on foraminifera, ostracoda, calcareous nannofossils and stable isotopes (δ13C, δ18O). Geologica Acta 7, 93–112.
Steurbaut, E., Sztrákos, K., 2008. Danian/Selandian boundary criteria and North Sea Basin-Tethys correlations based on calcareous nannofossil and foraminiferal trends in SW France. Marine Micropaleontology 67, 1–29.
Tawadros, E., 2001. The geology of Egypt and Libya. A.A. Balkema, Rotterdam, Brookfield. 472 pp.
Thomas, E., 1998. The biogeography of the late Paleocene benthic foraminiferal extinction. In: Aubry, M.-P., Lucas, S., Berggren, W.A. (Eds.), Late Paleocene-early Eocene Biotic and Climatic Events in the Marine and Terrestrial Records. Columbia University Press, pp. 214–243.
Thomas, E., Zachos, J.C., 2000. Was the late Paleocene thermal maximum a unique event? GFF 122, 169–170.
Thomas, D.J., Zachos, J.C., Bralower, T.J., Thomas, E., Bohaty, S., 2002. Warming the fuel for the fire: evidence for the thermal dissociation of methane hydrate during the Paleocene–Eocene thermal maximum. Geology 30, 1067–1070.
Thomson, J., Higgs, N.C., Wilson, T.R.S., Croudace, G.J., de Lange, G.J., van Santvoort, P.J.M., 1995. Redistribution and geochemical behaviour of redox-sensitive elements around S1, the most recent eastern Mediterranean sapropel. Geochimica et Cosmochimica Acta 59, 3487–3501.
Van der Zwaan, G.J., Jorissen, F.J., De Stigter, H.C., 1990. The depth dependency of planktonic/benthic foraminiferal ratios: Constraints and applications. Marine Geology 95, 1–16.
Van Morkhoven, F.P.C.M., Berggren, W.A., Edwards, A.S., 1986. Cenozoic Cosmopolitan Deep-Water Benthic Foraminifera. Elf Aquitaine, Pau.
Varol, O., 1989. Paleocene calcareous nannofossil biostratigraphy. In: van Heck, S.E. (Ed.), Nannofossils and their applications. Ellis Horwood Ltd., Chichester, pp. 267–310.
Wade, B.S., Pearson, P.N., Berggren, W.A., Pälike, H., 2011. Review and revision of Cenozoic tropical planktonic foraminiferal biostratigraphy and calibration to the geomagnetic polarity and astronomical time scale. Earth-Science Reviews 104, 111–142.
Westerhold, T., Röhl, U., Raffi, I., Fornaciari, E., Monechi, S., Reale, V., Bowles, J., Evans, H.F., 2008. Astronomical calibration of the Paleocene time. Palaeogeography, Palaeoclimatology, Palaeoecology 257, 377–403.
Westerhold, T., Röhl, U., Donner, B., McCarren, H., Zachos, J., 2011. A complete high-resolution Paleocene benthic stable isotope record for the Central Pacific (ODP site 1209). Paleoceanography. doi:10.1029/2010PA002092.
Wignall, P.B., Newton, R., 2001. Black shales on the basin margin: a model based on examples from the Upper Jurassic of the Boulonnais, northern France. Sedimentary Geology 144, 335–356.
Youssef, M.A., 2009. High resolution calcareous nannofossil biostratigraphy and paleoecology across the Latest Danian Event (LDE) in central Eastern Desert, Egypt. Marine Micropaleontology 72, 111–128.
Zachos, J.C., Dickens, G.R., Zeebe, R.E., 2008. An early Cenozoic perspective on greenhouse warming and carbon-cycle dynamics. Nature 451, 279–283.